Tesis

# CRITICAL CONDITION AND PHASE DIAGRAM IN THE NAMBU-JONA-LASINIO MODEL

PARA OBTENER EL TÍTULO DE

*DOCTOR EN CIENCIAS EN EL ÁREA DE FÍSICA*


*Presenta*

ANGELO MARTÍNEZ

*Asesor*

ALFREDO RAYA MONTAÑO

Instituto de Física y Matemáticas

Universidad Michoacana de San Nicolás de Hidalgo



Morelia, Michoacán. Marzo 2021

# PUBLICATIONS

This thesis is based upon the results of the following articles, out of which some of the figures were taken:


[1] Angelo Martínez and Alfredo Raya. An innovative approach for sketching the qcd phase diagram within the njl model using lagrange multipliers, 2019. arXiv: 1909.12416 [hep-ph].

[2] Aftab Ahmad, Angelo Martínez, and Alfredo Raya. Superstrong coupling njl model in arbitrary spacetime dimensions. *Physical Review D*, 98(5), September 2018. DOI: 10.1103/physrevd.98.054027. URL: http://dx.doi.org/10.1103/PhysRevD.98.054027.

[3] A. Martinez and A. Raya. On the iterative solution of the gap equation in the Nambu-Jona-Lasinio model. *J. Phys. Conf. Ser.*, 912(1):012010, 2017. I. Bautista, E. de la Cruz Burelo, A. Fernández-Téllez, G. López-Castro, M. Rodrıguez-Cahuantzi, and P. Roig, editors. DOI: 10.1088/1742-6596/912/1/012010.

[4] Angelo Martınez and Alfredo Raya. Critical chiral hypersurface of the magnetized NJL model. *Nucl. Phys. B*, 934:317–329, 2018. DOI: 10.1016/j.nuclphysb.2018.07.008. arXiv: 1804.03183 [hep-th].

# CONTENTS

1 INTRODUCTION 1

The NJL model

2 THE NJL MODEL AND THE GAP EQUATION 5
- 2.1 The two flavor NJL model 6
- 2.2 The gap equation in vacuum 7
- 2.3 Regularization schemes 8
- 2.4 Parameter fixing and solutions 11
- 2.5 Introducing temperature 14
- 2.6 Gap equation in a medium 16

The Critical condition

3 THE PHASE DIAGRAM OF THE NJL MODEL 23
- 3.1 The phase-diagram of the NJL model 24
- 3.2 Thermodynamic potential 26
- 3.3 The gap equation from thermodynamic potential 28
- 3.4 Critical coupling in vacuum 28
- 3.5 Critical coupling in a thermal bath 32
- 3.6 Critical coupling in a hot and dense medium 34
- 3.7 Lagrange Multipliers and the gap equation 37
- 3.8 From the critical coupling to the phase-diagram 38

Using the critical condition

4 THE CRITICAL CONDITION IN ACTION 43
- 4.1 Critical coupling: magnetic and thermal contribution 43
- 4.2 Critical coupling: thermo-magnetic contribution 48
- 4.3 Critical coupling in arbitrary dimensions 48
- 4.4 The phase diagram of the NJL model 51
- 4.5 Phase diagram - the medium contribution 53
- 4.6 Phase diagram - $T_c$ and $\mu_c$ as boundaries 56

Conclusions
5 CONCLUSIONS 61
Bibliography 63

# LIST OF FIGURES


Figure 2.1 Schwinger-Dyson equation for the quark propagator in the Hartree approximation. The dressed (bare) propagator is denoted by the bold (thin) line. 7

Figure 2.2 Contour to carry out the integral in Eq. (2.6). 9

Figure 2.3 Solution for the dimensionless gap equation for the $3D$ cutoff regularization scheme. 13

Figure 2.4 Solution for the dimensionless gap equation for $3D$cutoff regularization scheme. 14

Figure 2.5 Contour to carry out the summation in Eq. (2.27). 17

Figure 3.1 Sketch of the QCD phase-diagram. 24

Figure 3.2 Schematics of heavy ion-collision. In this picture the squashed ions gets closer to each other in a) and b) then they pass each other in c). Finally, the system expands, cools down and hadronizes d). 25

Figure 3.3 Determination of a second order phase boundary using the thermodynamic potential. Note how the minimum moves to the $m = 0$ axis. 27

Figure 3.4 Determination of a first order phase boundary using the thermodynamic potential. Note how the minimum moves toward the $m = 0$ axis. 29

Figure 3.5 Plot of the solutions of Eq. (3.3) as a function of the coupling constant. It is easy to see that the coupling strength needed to trigger the formation of the chiral condensate increases as temperature raises. The equation was solved iteratively as described in [10]. $\mu = 0$ for all cases. 30

Figure 3.6 Plot of the right hand side and left hand side of the gap equation, Eq. (3.4), for various values of the coupling constant. 31

Figure 3.7 Plot of the right hand side and left hand side of the gap equation, Eq,. (3.8), for various values of the coupling constant. $T = 0.13$ GeV in all plots. 33
Figure 3.8 Critical coupling of the NJL model on a thermal bath. The regularization parameter $\Lambda = 0.942$ GeV. 35
Figure 3.9 Plot of Eqs. (3.11) for various values of the coupling. The inclusion of the chemical potential makes the black curve to develop a concavity. 36
Figure 3.10 Plot of all the values $(G_i, T_i, \mu_i)$ obtained from the critical condition Eq. (3.15). The regularization parameter was fixed at $\Lambda = 0.942\,\text{GeV}$. 39
Figure 4.1 Critical coupling for the proper time regulated gap equation in a thermal bath. Notice the limiting temperature $T_L$. 45
Figure 4.2 Plot of the mass function for the gap Eq. (4.2) with $T = 0$ for various values of the magnetic field. $\Lambda = 4.66 \times 10^{-1}$ GeV$^{-2}$. Notice the steep increase in the value of the mass. 46
Figure 4.3 Plot of the pseudo-critical coupling defined as the coupling from which the generated mass exceeds $m \geq 10^{-4}\,\text{GeV}$. 47
Figure 4.4 Critical coupling for the gap equation, Eq. (4.2), for various values of the magnetic field strength. 49
Figure 4.5 Plot of the critical coupling for the NJL model and the CI model as a function of the number of dimensions for the parameters shown in Table I in Ref. [3]. 50
Figure 4.6 Comparison of the critical coupling for the NJL model in vacuum for various dimensions. Note that the necessary coupling in $D = 2$ is zero. 51
Figure 4.7 Comparison of the critical coupling for the CI model in vacuum for several dimensions. 52
Figure 4.8 Plot of the critical coupling as a function of temperature and chemical potential obtained after differentiating the solutions (one or two) of Eq. (3.15) and then plugging in the values of $T$, $\mu$ and $m$ into the gap equation Eq. (2.31) to get the critical coupling. The regularization parameter $\Lambda = 0.942\,\text{GeV}$. To draw the actual phase diagram, we slice Fig. 4.8 in the desired value of the coupling. 54

Figure 4.9 Phase diagram obtained after slicing Fig. 4.8 for $G = 2.6$ GeV$^{-2}$, $G = 3.0$ GeV$^{-2}$ and $G = 3.5$ GeV$^{-2}$. The orange area shows the second phase transition zone, whereas the gray area shows the first order phase transition zone. Notice how as the coupling becomes larger the first phase transition zone "wraps" around the second phase transition zone. 55

Figure 4.10 Plot of the critical coupling for the gap equation Eq. (2.31) with the medium integrals regularized. $\Lambda = 0.942$ GeV. 56

Figure 4.11 Phase diagram obtained after slicing Fig. 4.10 with $G = 2$ GeV$^{-2}$, $G = 3$ GeV$^{-2}$ and $G = 3.5$ GeV$^{-2}$. In the mid plot, $T_c \approx 0.411$ GeV and $\mu_c \approx 0.737$ GeV whereas the CEP is located at $T_{CEP} \approx 0.225$ GeV and $\mu_{CEP} \approx 0.49$ GeV. For the lower plot, $T_c \approx 0.513$ GeV and $\mu_c \approx 0.94$ GeV and the CEP is located at $T_{CEP} \approx 0.3$ GeV and $\mu_{CEP} \approx 0.56$ GeV. 57

Figure 4.12 Phase diagram obtained fixing $T_c = 0.186$ GeV and $\mu_c = 0.323$ GeV in Eq. (3.15). After solving, $\Lambda = 0.8$ GeV and $G = 3.072$ GeV$^{-2}$ and the CEP is located $T_{CEP} = 0.049$ GeV and $\mu_{CEP} = 0.31$ GeV. 58

## LIST OF TABLES

Table 2.1 Symmetries of the NJL model. 6

Table 2.2 Parameters for the $3D$ cutoff. Taken from [8]. 12

Table 2.3 Parameters for proper time regularization. Taken from [8]. 12

# ABSTRACT

The theory that describes the dynamics of quarks and gluons is the theory of Quantum Chromodynamics (QCD). It is well known that all the perturbative methods developed to study Quantum Electrodynamics can only used at high energies in QCD. To study low energy phenomena it is necessary to use non-perturbative methods as LatticeQCD, Schwinger-Dyson equations, chiral perturbative theory, effective models, among others.

One of the scenarios in which the picture drawn by the perturbative approaches is not complete is in the exploration of the phase diagram of QCD. Here the effects of temperature and chemical potential must be taken into account to effectively describe how the QCD matter behaves under extreme circumstances. LatticeQCD, being a first principles approach to QCD, regularly comes as the tool that set the bar for theoretical approaches. Nonetheless, in the problem of sketching the phase diagram, it gets limited by the sign problem when chemical potential is taken into account. In this sense, there is still a need for the development of new theoretical approaches to study QCD and in this case the phase diagram.

In this thesis we use the Nambu-Jona-Lasinio (NJL) model to explore the phase diagram of QCD. We found conditions from which the breaking of the chiral symmetry gets trigger as a function of the medium and the model parameters.

# RESUMEN

La teoría que describe la dinámica de quarks y gluones es la Cromo Dinámica Cuántica (QCD). Como es bien sabido todas las técnicas perturbativas desarrolladas para el estudio de la Electrodinámica Cuántica sólo son aplicables a QCD en el régimen de altas energías. Para fenómenos a bajas energías es necesario usar métodos no perturbativos como lo son LatticeQCD, ecuaciones de Schwinger-Dyson, teoría perturbativa quiral, modelos efectivos, entre otros.

Uno de los escenarios en donde las técnicas perturbativas no dan la imagen completa, es en la exploración del diagrama de fase de QCD. Aquí, los efectos de la temperatura y el potencial químico deben ser tomados en cuenta para poder describir como la materia nuclear se comporta en condiciones extremas.

Dado que LatticeQCD estudia QCD desde primeros principios, es la herramienta de comparación principal para los métodos teóricos. Sin embargo cuando se agrega el potencial químico, LatticeQCD se ve limitado en la descripción del diagrama de fase por el problema del signo. En este sentido existe la necesidad de desarrollar nuevos métodos para estudiar QCD, y en este caso, el diagrama de fase.

En esta tesis empleamos el modelo de Nambu-Jona-Lasinio (NJL) para explorar el diagrama de fases efectivo de QCD. Se encontraron condiciones para las cuales se lleva a cabo el rompimiento de simetría quiral como función de los parámetros del medio y del modelo.

Palabras clave: QCD, Diagrama de Fases, Simetría quiral, Modelo NJL, Ecuación de gap.

# 1

# INTRODUCTION

The modern theory that describes the dynamics of quarks and gluons is Quantum Chromodynamics (QCD), and even though it has seen a growing success since its formulation in the early 1970s, it has posed a huge amount of challenges for the scientific community. QCD is successful in the description of the phenomena of confinement and asymptotic freedom. The former states that at low momentum, quarks always form composed states named hadrons, whereas the latter tells us that at high momentum, the constituent quarks behave as free particles. As we stated before, QCD presented a huge amount of challenges to the scientific community. On one hand, QCD incorporates gluons, the gauge bosons that transmit the strong force, and unlike the photons in the electromagnetic interactions, gluons have self interactions. This adds a huge complexity to the Feynman Diagrams that must be calculated to study a certain processes. On the other hand, the phenomenon of asymptotic freedom tells us that all the perturbative approaches developed from the study of Quantum Electrodynamics can only be used at high energies studies in QCD. This means that all the low energies phenomena in QCD must be studied using non-perturbative approaches, such as LatticeQCD, Schwinger-Dyson equations, chiral perturbative theory, effective models, among others. An interesting feature of QCD is the explanation of the phenomenon of dynamical mass generation. This mechanism is the responsible of above 90% of the observable mass of the universe.

One of the scenarios in which the picture drawn by the perturbative approaches is not complete is in the exploration of the phase diagram of QCD. In this scenario, the effects of temperature and chemical potential must be taken in to account to effectively describe how the QCD matter behaves under extreme circumstances. LatticeQCD, being a first principles approach to QCD, regularly comes as the tool that set the bar for theoretical approaches. Nonetheless, in the problem of sketching the phase diagram, it gets limited by the sign problem when chemical potential is taken into account. In this sense, there is still a need for the development of new theoretical approaches to study QCD and in this case the phase diagram.

To study the phase diagram of QCD, in this thesis we resort to the Nambu-Jona-Lasinio (NJL) model. The NJL model was one of the first attempts to describe strong interactions. Introduced as a point interaction before the formulation of QCD, it is able to gasp some robust aspects of the full theory, like the chiral symmetry breaking phenomenon that give rise to dynamical generation of mass.

This thesis is organized as follows: In Chapter 1 we introduce the basic properties of the NJL model, obtain the gap equation for various regularization procedures and introduce a dense heat bath necessary ingredients to explore the phase diagram. In Chapter 2 the phase diagram of QCD is introduced. In order to depict it from the NJL model we obtain the same gap equation as before from the thermodynamic potential. It is here where we introduce the critical coupling $G_c$ necessary to break chiral symmetry in the model and then generalize the concept using Lagrange Multipliers to finally obtain the critical condition that is used in Chapter 3, where we obtain the critical coupling for the gap equation under various medium conditions. Then, we finally exploit the critical condition from Chapter 2 to sketch the phase diagram of the NJL model and get the location of the critical end point (CEP). At the end, in Chapter 4, we present the conclusions of the thesis.

# THE NJL MODEL

# 2

# THE NJL MODEL AND THE GAP EQUATION

In order to explain the strong interactions, one of the first models was proposed by Nambu and Jona-Lasinio in 1961, dubbed the NJL model [1, 2]. Even though nowadays we have the theory of Quantum Chromodynamics (QCD) that describes with high precision the interactions of quarks and gluons. Unlike Quantum Electrodynamics (QED) in which at low energies the strength of the interactions decreases, in QCD the opposite occur. At high energies, the strength of the interactions become weaker due to the phenomenon of asymptotic freedom and thus the theory can be studied with the perturbative methods already developed for QED at high precision. In the other side of the spectrum, at low energies, the interactions becomes stronger, and thus, the theory becomes highly nonlinear, which render getting any precise calculations a really hard task. One of the main advantages of the NJL model is that even though simple, it is capable of capturing some robust characteristics of the strong interactions in the infrared regime ($\approx$ 1 GeV), whereas in the ultraviolet regime it fails as the model was devised before the discovery of the quarks and the phenomenon of confinement. Historically the NJL model describes fermions that interact at contact in analogy with the Cooper pairs in the Bardeen–Cooper–Schrieffer (BCS) theory of superconductivity. The success of the model is the description of the phenomenon of chiral symmetry breaking and dynamical mass generation, that as we now know, it is the responsible for approximately $\approx$ 97% of the mass of the proton. Nowadays, the NJL model is regarded as a low energy approximation to QCD with point interactions between quarks without gluons. As such, the model doesn't describe confinement. It can be (weekly) achieved by removing the poles of the propagator [3], coupling it to a Polyakov loop trough an effective potential [4] or making the interaction non-local [5]. The main interest in this thesis is the study of the phase diagram of QCD and, by taking advantage of the simplicity of the NJL model, introduce a new method based in Lagrange multipliers that simplifies the process of depicting the phase diagram.

| Symmetry | Transformation | Current | Conserved Charge |
|---|---|---|---|
| $U_V(1)$ | $\psi \to e^{-i\alpha}\psi$ | $j_\mu = \bar{\psi}\gamma_\mu\psi$ | Baryonic number |
| $SU_v(2)$ | $\psi \to e^{-i\tau\cdot\omega/2}\psi$ | $J^k_\mu = \bar{\psi}\gamma_\mu\tau^k\psi$ | Isospin |
| $SU_A(2)$ | $\psi \to e^{-i\tau\cdot\theta\gamma^5/2}\psi$ | $J^k_\mu = \bar{\psi}\gamma_\mu\gamma^5\tau^k\psi$ | Chiral symmetry |

Table 2.1: Symmetries of the NJL model.

In this Chapter we introduce the NJL model and derive the gap equation that allow us to study the phenomenon of chiral symmetry breaking.

## 2.1 THE TWO FLAVOR NJL MODEL

The Lagrangian of the two flavor NJL model has the basic structure

$$\mathcal{L} = \bar{\psi}(i\not{\partial} + m_q)\psi + G\left\{(\bar{\psi}\psi)^2 + \left(\bar{\psi}i\gamma^5\vec{\tau}\psi\right)^2\right\}, \tag{2.1}$$

where $\psi$ is the quark field, $m_q$ is the current quark mass, $\vec{\tau}$ are the Pauli matrices acting on the isospin space and $G$ is the coupling constant. The modern interpretation of the model was constructed with the symmetries shown in Table 2.1. Originally a $U_A(2)$ symmetry was also considered but it was later discarded in accordance to experimental observations. Given the absence of gluons, the interactions are punctual and as such, the model is not renormalizable with nonremovable divergences that need to be regularized with a regularization scheme that depends upon a parameter.

As was mentioned before, the success of the NJL model is that is capable of describing the chiral symmetry breaking that leads to the phenomenon of dynamical mass generation. This breaking of the chiral symmetry is due to the condensation of a pair quark antiquark (chiral condensate). This pairing akin to the Cooper pair in the BCS theory is responsible of giving rise to a constant dynamical mass that appear even if no current quark mass is present $m_q = 0$. For a more in depth review of the NJL model, its applicability in hadronic matter and the three flavor NJL model refer to [6, 7].

To see explicitly this process of pairing, we need to derive from Eq. (2.1) the so called gap equation.

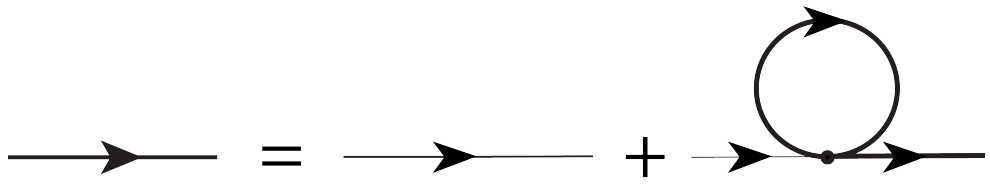

Figure 2.1: Schwinger-Dyson equation for the quark propagator in the Hartree approximation. The dressed (bare) propagator is denoted by the bold (thin) line.

## 2.2 THE GAP EQUATION IN VACUUM

Now we turn to our main object of study in this thesis, the gap equation. The gap equation is the relation obtained when we minimize the total energy of the system. One way to get the gap equation is to use the Schwinger-Dyson equations in the Hartree approximation for the quark propagator that we can see in Fig. 2.1. In this approximation, the self-consistent gap equation takes the form

$$m = m_q - 2G\langle\bar{\psi}\psi\rangle, \tag{2.2}$$

where $m$ is the dynamically generated mass, $m_q$ is the current quark mass, $G$ is the coupling constant and $\langle\bar{\psi}\psi\rangle$ is the chiral condensate, the order parameter associated with the chiral symmetry, defined as

$$-\langle\bar{\psi}\psi\rangle = \int \frac{d^4k}{(2\pi)^4} Tr\left[iS(k)\right]. \tag{2.3}$$

Here the trace is over flavor and color spaces and $S(k)$ is the dressed quark propagator[1]

$$S(k) = \frac{(\not{k} + m)}{k^2 - m^2}. \tag{2.4}$$

1 Even though the fermion propagator should have a renormalization of the wave function and a mass renormalization terms, it can be shown that in the NJL model these terms can be neglected as they turn out to be constants.

As we can appreciate, Eq. (2.2) does not depend on the external momentum, and therefore it is just a constant that shifts the pole of the propagator. The symmetry is broken whenever the chiral condensate acquire a non-zero value. This occurs after the coupling constant $G$ surpasses a certain critical value $G_c$. What remain is to perform the integrals in Eq. (2.3) that must be regularized.

## 2.3 REGULARIZATION SCHEMES

There are several ways to regularize the integrals in Eq. (2.3), from non-covariant methods like a hard cutoff in the spatial momentum, covariant methods like 4-momentum cutoff, Pauli-Villars regularization, the latter based on adding a "drag" term to the propagator, proper time regularization and dimensional regularization. For an in depth analysis of each method mentioned, please refer to [8]. For the purposes of this thesis, we adopt the 3-momentum cutoff and proper time regularizations.

### *3D cutoff*

We begin with the 3D cutoff in the momentum. The main idea is to add an infrared cutoff to the integral. We start with the chiral condensate Eq. (2.3)

$$\begin{aligned}\langle\bar{\psi}\psi\rangle &= -\int \frac{d^4k}{(2\pi)^4} Tr\left[iS(k)\right] \\ &= -4N_f N_c i\, m \int \frac{d^4k}{(2\pi)^4} \frac{1}{k^2 - m^2} \\ &= -4N_f N_c i\, m\, I\left(m\right), \end{aligned} \tag{2.5}$$

with the constants $N_f$ and $N_c$ representing the number of fermions and colors respectively; as we are working with the two flavor NJL model, $N_f = 2$ and $N_c = 3$. Out next goal is to perform the integral $I\left(m\right)$, defined as

$$I\left(m\right) = \int \frac{d^4k}{(2\pi)^4} \frac{1}{k^2 - E_k^2}, \tag{2.6}$$

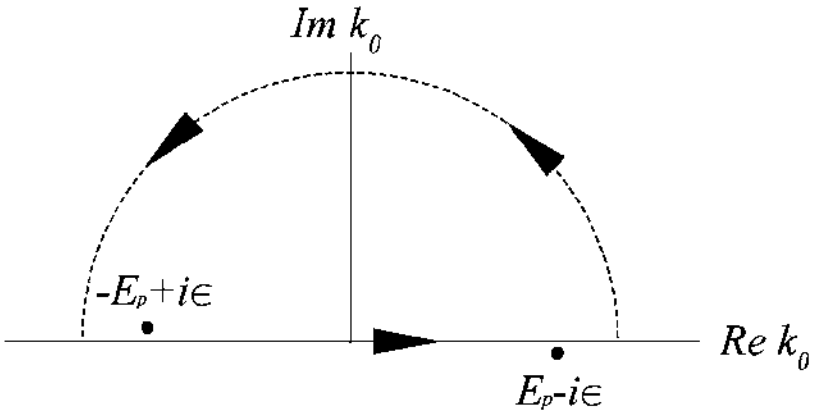


Figure 2.2: Contour to carry out the integral in Eq. (2.6).

where $E_k = \sqrt{\vec{k}^2 + m^2}$. The first step is to carry out the integral along the $k_0$ momentum using the residue theorem and the path shown in Fig. 2.2. Then,

$$\int_{-\infty}^{\infty} dk_0 \frac{1}{k_0^2 - E_k^2} = -\frac{i\pi}{E_k}.$$

Next, we switch to spherical coordinates and introduce our ultraviolet cutoff $\Lambda_{3D}$ in the radial integral. Upon carrying out the remaining of the integral,

$$\frac{-i\pi}{(2\pi)^4}\int_{\Lambda_{3D}} d^3k \frac{1}{\sqrt{\vec{k}^2+m^2}} = -\frac{i4\pi^2}{(2\pi)^4}\frac{1}{2}\left\{\Lambda_{3D}\sqrt{\Lambda_{3D}^2+m^2} - m^2 \ln\left(\frac{\Lambda_{3D}+\sqrt{\Lambda_{3D}^2+m^2}}{m}\right)\right\}. \quad (2.7)$$

Finally, combining Eq. (2.7) and Eq. (2.2) the gap equation takes the form

$$m = m_q + m\frac{GN_fN_c}{\pi^2}\left\{\Lambda_{3D}\sqrt{\Lambda_{3D}^2+m^2} - m^2 \ln\left(\frac{\Lambda_{3D}+\sqrt{\Lambda_{3D}^2+m^2}}{m}\right)\right\}. \quad (2.8)$$

A few notes about Eq. (2.8) are at hand:

- The gap equation is in nature a self-consistent and transcendental relation among the parameters of the model, making it highly non-linear.
- Without medium effects, the dynamical mass $m$ can have up to three values, the trivial one $m = 0$ and two non zero values $m > 0$ and $m < 0$, depending on the parameters $G$ and $\Lambda_{3D}$.
- For hadronic studies purposes, the free parameters $G$ and $\Lambda_{3D}$ are fixed by using the experimental value for the pion decay constant $f_\pi$ and the value for the quark condensate per flavor $\langle \bar{q}q \rangle$. In later Chapters we use some of the fitted values to compare with our results. For more details about the fitting process, see [7, 8].

*Proper time*

The proper time regularization is based on the relation

$$\frac{1}{a+ib} = \int_0^\infty ds\, e^{-(a+ib)s}, \tag{2.9}$$

for $a,\ b \in \mathbb{R}$ and $a > 0$. Then we apply it to the propagator. In Eq. (2.6) after a Wick rotation $k_0 \to -ik_0$. The exponential term allows us compute all the momentum integral with ease, each one contributes with a factor of $\sqrt{\frac{\pi}{\tau}}$. This lead us to

$$I(m) = \frac{\pi^2}{(2\pi)^4} \int \frac{ds}{s^2} e^{-m^2 s}. \tag{2.10}$$

Finally, the gap equation reads

$$m = \frac{GN_f N_c}{2\pi^2} m \int_0^\infty ds \frac{e^{-m^2 s}}{s^2}. \tag{2.11}$$

It is in this point where we add the regularization parameter $\Lambda_{PT}$ as an infrared cutoff in the proper-time. Then,

$$m = \frac{GN_f N_c}{2\pi^2} m \int_{\Lambda_{PT}}^\infty ds \frac{e^{-m^2 s}}{s^2} = \frac{e^{-m^2 \Lambda_{TP}}}{\Lambda_{TP}} - m^2 \Gamma\left(0, m^2 \Lambda_{TP}\right), \tag{2.12}$$

where $\Gamma(a,z)$ is the incomplete gamma function, defined as

$$\Gamma(a,z) = \int_z^\infty dt\, t^{a-1} e^{-t}. \tag{2.13}$$

We should point out that unlike the 3D cutoff regularization, the proper time method preserves Lorentz symmetry even though in both cases the inclusion of the temperature breaks it anyway.

## 2.4 PARAMETER FIXING AND SOLUTIONS

For purposes of comparison, we need to fix $\Lambda$ and $G$. This is done by using the pion decay constant $f_\pi$, known from measurements of the decay $\pi^- \to \mu^- + \nu_\mu$ and the mass of the pion $m_\pi$.

The pion decay constant $f_\pi$ takes the form

$$f_\pi^2 = \begin{cases} \frac{N_c m^2}{(2\pi)^3} \int^{\Lambda_{3D}} d^3k \frac{1}{E_k^3}, & 3D \text{ cutoff}, \\ \frac{N_c m^2}{4\pi^2} \int_{m^2/\Lambda_{PT}^2}^\infty ds \frac{e^{-s}}{s}, & \text{proper time}, \end{cases}$$

whereas the pion mass can be obtained from the expression

$$\left[1 - 2G\Pi^\pi(p^2)\right] |_{p^2=m_\pi^2} = 0, \tag{2.14}$$

where

$$\Pi^\pi(p^2) = 2i \int \frac{d^4k}{(2\pi)^4} tr\left[\gamma_5 S(k) \gamma_5 S(k-p)\right], \tag{2.15}$$

is calculated in the appropriate regularization. Common values for the decay constant are $f_\pi = 94$ MeV and for the pion mass are $m_\pi = 135$ MeV .

In Table 2.2 and 2.3 we show some values for the parameters $\Lambda$ and $G$.

Because of its non-linear nature, the gap equation can not be solved in a closed form, but it can be solved numerically, nonetheless, using iterations [9][10]. An example of the solution for $3D$ cutoff regularization can be seen in Fig. 2.3. We can see the

| $m_u$ (MeV) | $\Lambda_{3D}$ (MeV) | $G\,10^{-6}$ (MeV$^{-2}$) | $m$ (MeV) | $\langle\bar{u}u\rangle^{1/3}$ (MeV) |
|---|---|---|---|---|
| 3.0 | 942 | 2.00 | 220 | $-300$ |
| 4.0 | 781 | 3.09 | 225 | $-272$ |
| 5.0 | 665 | 4.71 | 311 | $-253$ |
| 5.5 | 609 | 6.26 | 375 | $-245$ |

Table 2.2: Parameters for the $3D$ cutoff. Taken from [8].

| $m_u$ (MeV) | $\Lambda_{PT} \cdot 10^{-5}$ (MeV$^{-2}$) | $G\,10^{-6}$ (MeV$^{-2}$) | $m$ (MeV) | $\langle\bar{u}u\rangle^{1/3}$ (MeV) |
|---|---|---|---|---|
| 3.0 | 466 | 1.61 | 178 | $-300$ |
| 5.0 | 830 | 3.07 | 204 | $-253$ |
| 10.0 | 17 | 8.13 | 265 | $-198$ |

Table 2.3: Parameters for proper time regularization. Taken from [8].

solution for the gap equation Eq. (2.8) after taking the chiral limit $m_u \to 0$ and being cast into dimensionless form by redefining

$$\begin{aligned} m &\to M = \frac{m}{\Lambda_{3D}}, \\ G &\to G' = \frac{N_f N_c}{\pi^2} G \Lambda_{3D}^2, \end{aligned} \tag{2.16}$$

for the $3D$ cutoff regularization and

$$\begin{aligned} m &\to M^2 = m^2 \Lambda_{PT}, \\ G &\to G' = \frac{N_f N_c}{2\pi^2} G \Lambda_{PT}, \end{aligned} \tag{2.17}$$

for proper time regularization.

From Fig. 2.3 we can see the various features of the gap equation. On one hand the phenomenon of chiral symmetry breaking is obvious; at $G' = 1$, the generated mass becomes non-zero, as expected because the coupling becomes strong enough to enable the formation of the chiral condensate. It should be pointed out that the gap equation has multiple solutions, depending on the set of parameters chosen and

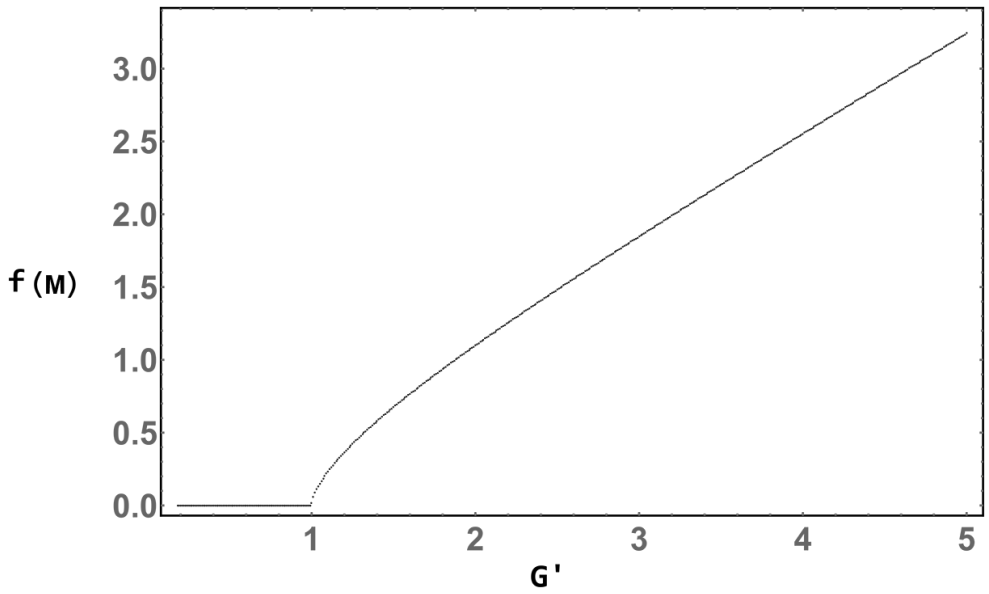


Figure 2.3: Solution for the dimensionless gap equation for the $3D$ cutoff regularization scheme.

$M = 0$ is still a solution for all values of the coupling but for $G' \geq 1$, it becomes unstable and the non-zero solution becomes the stable one. On the other hand, the generated mass grows approximately linear on the coupling, as we see shortly, this is not an universal feature of Eq. (2.8) and depends on the regularization scheme.

Now we can turn our attention to Fig. 2.4 and as in the previous case, there is a critical coupling from which the dynamical mass begins being generated. We can see that the growing of the dynamical mass with respect to the coupling is approximately logarithmic, in contrast with the $3D$ cutoff. Another feature that pops to the eye is that at large coupling $G'3.73$, for example $G' = 1 = G'_c$ transform to $G_c = 3.06 \cdot 10^{-6}\text{MeV}^{-2}$, the iteration procedure develops bifurcations meaning that the solution isn't stable. It should be stressed that this behavior is found on the proper time and Pauli-Villars regularizations only [11].

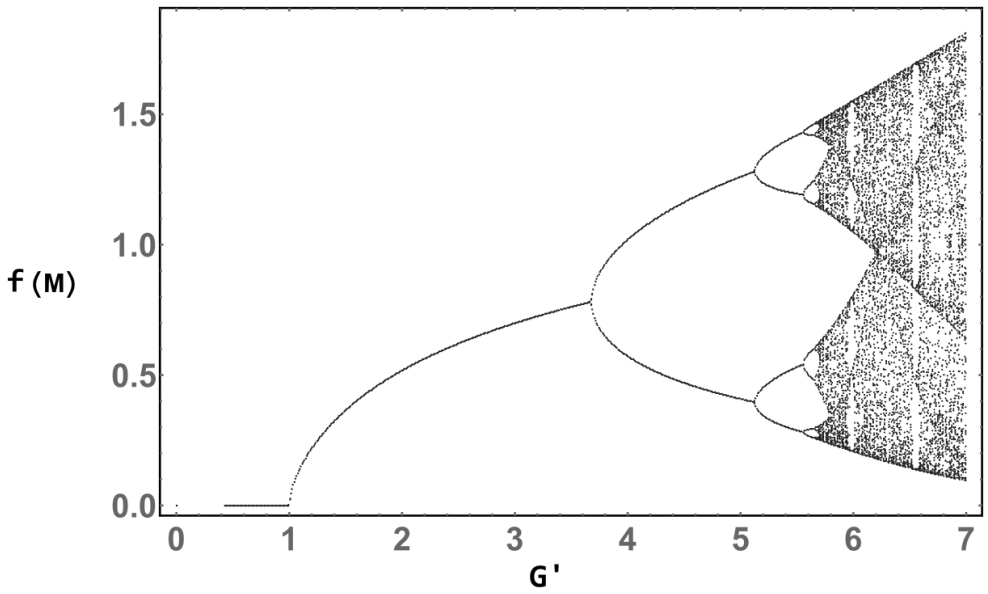


Figure 2.4: Solution for the dimensionless gap equation for 3$D$cutoff regularization scheme.

## 2.5 INTRODUCING TEMPERATURE

Before proceeding any further, we need to introduce the effects of a heat bath into the gap equation. The intuition for a thermal bath is; a medium that excites the particles you put in, for us the quarks. Such a medium has a noticeable effect on the breaking of the chiral symmetry. Usually, the effect is to restore the chiral symmetry and the mass formation.

One of the many ways to introduce the effects of a thermal bath is to use the Matsubara formalism of imaginary time [12–15]. Here we take advantage of the similarities between the transition amplitude in QFT at zero temperature and the partition function. Recalling the transition amplitude from QFT

$$Z[J] = \langle \phi_1 \mid e^{-iH(t_1 - t_2)} \mid \phi_2 \rangle = \int \mathcal{D}\phi e^{iS[x,J]}, \tag{2.18}$$

where $S[x, J]$ is the action defined as

$$S[x, J] = \int d^4x \left[\mathcal{L} + J(t)\, x(t)\right], \tag{2.19}$$

and $J(t)$ is a classical source. The partition function for any quantum system is

$$Z[\beta] = Tr\, e^{-\beta\mathcal{H}} = \int d\phi_1 \langle \phi_1 \mid e^{-\beta\mathcal{H}} \mid \phi_1 \rangle, \tag{2.20}$$

where we have identified $t_1 - t_2 = -i\beta$. Then, it follows that we can give the partition function a path integral representation

$$Z[\beta] = N' \int \mathcal{D}\phi\, e^{-\mathcal{S}_E}. \tag{2.21}$$

Here $S_E$ is the Euclidean action. For a fermion and a non-zero chemical potential $\mu$,

$$\mathcal{S}_E = \int_0^\beta d\tau \int d^3x \bar{\psi} \left[\gamma^\mu \partial_\mu - \gamma_0 \mu + m\right] \psi. \tag{2.22}$$

It is worth noting that in Eq. (2.20) the initial and final states are the same; this comes from the trace of the partition function. Furthermore the (fermionic) bosonic field $\phi$ satisfies the (anti)periodic conditions

$$\phi_1(x, 0) = \pm\phi_1(x, \beta). \tag{2.23}$$

Condition Eq. (2.23) together with Eq. (2.22) have as a consequence that the propagator becomes dependent on a discrete variable $\omega_n + i\mu$, thus

$$\mathcal{G}_\beta\left(\omega_n, \vec{k}\right) = \frac{1}{\left(\omega_n + i\mu\right)^2 + \vec{k}^2 + m^2}, \tag{2.24}$$

where the (anti)periodic conditions yield [12, 14]

$$\omega_n = \begin{cases} 2\pi n T, & \text{bosons,} \\ (2n+1)\,\pi T, & \text{fermions,} \end{cases} \tag{2.25}$$

with Eq. (2.24) and Eq. (2.25) it is straightforward to add the effects of the temperature to any gap equation.

## 2.6 GAP EQUATION IN A MEDIUM

Let us start with $3D$ cut off regularization. The first step is to perform the substitutions

$$\begin{aligned} k &\rightarrow \left(\omega_n + i\mu, \vec{k}\right), \\ \int \frac{dk_0}{2\pi} &\rightarrow T \sum_{n=-\infty}^{\infty}, \end{aligned} \tag{2.26}$$

to Eq. (2.6) and the last substitution comes from the finite limit of integration imposed on Eq. (2.22). Then, after a Wick rotation, Eq. (2.6) becomes

$$I(m) = iT \sum_{n=-\infty}^{\infty} \int \frac{d^3k}{(2\pi)^3} \frac{1}{(\omega_n - i\mu)^2 + E_k^2}. \tag{2.27}$$

The last summation can be done using the residue theorem with the contour shown in Fig. 2.5 and a auxiliary function

$$f(k_0) = \frac{1}{2} \tanh\left[\frac{(k_0 - \mu)}{2T}\right]. \tag{2.28}$$

We now note that $f(k_0)$ has simple poles in $k_0 = i\omega_n + \mu$ and unit residue. Then, we can rewrite the summation in Eq. (2.27) as the integral of $f(k_0)$

$$T\sum_n \frac{1}{(\omega_n - i\mu)^2 + E_k^2} = -\int_{\mathcal{C}} \frac{dk_0}{2\pi i} g(k_0) f(k_0) = -\int_{\mathcal{C}} \frac{dk_0}{2\pi i} g(k_0) \frac{1}{2} \tanh\left[\frac{k_0 - \mu}{2T}\right], \tag{2.29}$$

where $\mathcal{C} = \mathcal{C}_1 \cup \mathcal{C}_2$ and $g(k_0) = \frac{1}{\omega^2 - E_p^2}$. The contour integral can be written as the sum of the residues of $g(k_0)$ by closing the curves $\mathcal{C}_1$ and $\mathcal{C}_2$ with two semi-circles that enclose the poles of $g(k_0)$. Thus

$$\begin{aligned} T\sum_n g(k_0) f(k_0) &= -\frac{1}{2}\left[\frac{1}{2E_p} \tanh\left(\frac{E_k - \mu}{2T}\right) + \frac{1}{2E_p} \tanh\left(\frac{E_k + \mu}{2T}\right)\right]. \\ &= -\frac{1}{2}\left[\frac{1}{2E_k}\left(1 - \frac{2}{e^{\frac{E_k - \mu}{T}} + 1}\right) + \frac{1}{2E_p}\left(1 - \frac{2}{e^{\frac{E_k + \mu}{T}} + 1}\right)\right] \\ &= -\frac{1}{2}\left[\frac{1}{E_k} - \frac{1}{E_k}\frac{1}{e^{\frac{E_k - \mu}{T}} + 1} - \frac{1}{E_k}\frac{1}{e^{\frac{E_k + \mu}{T}} + 1}\right]. \end{aligned} \tag{2.30}$$

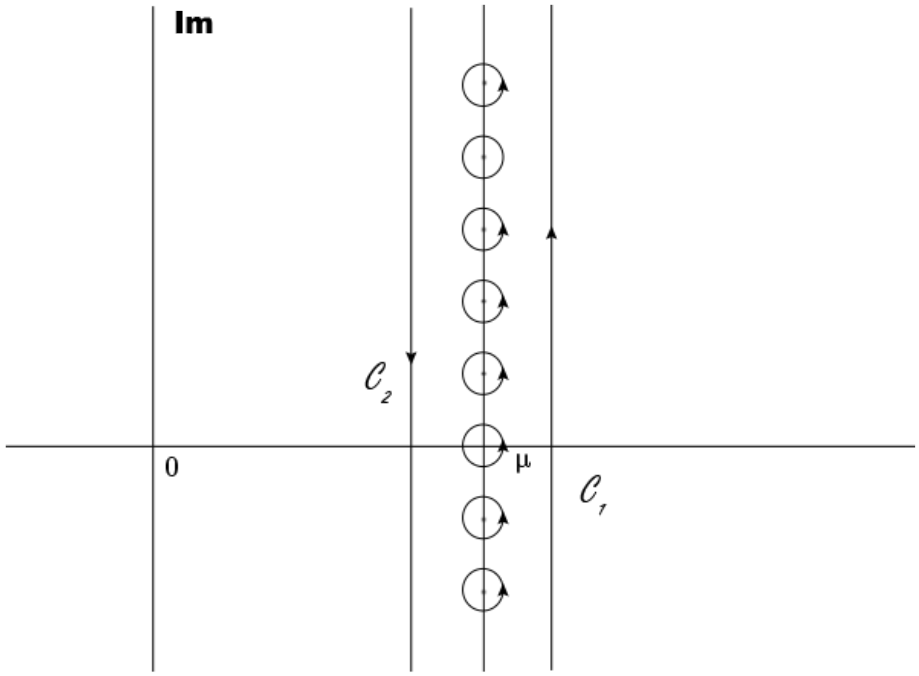


Figure 2.5: Contour to carry out the summation in Eq. (2.27).

Gathering results, the gap equation becomes

$$m = m_q + 4N_f N_c G\, m \int \frac{d^3k}{(2\pi)^3} \frac{1}{E_k} \left(1 - n_p\left(T,\mu\right) - \bar{n}_p\left(T,\mu\right)\right), \tag{2.31}$$

where $n_p$ and $\bar{n}_p$ are the Fermi occupation numbers of quarks and anti-quarks, respectively

$$\begin{aligned} n_p\left(T,\mu\right) &= \frac{1}{e^{\frac{E_p-\mu}{T}}+1}, \\ \bar{n}_p\left(T,\mu\right) &= \frac{1}{e^{\frac{E_p+\mu}{T}}+1}. \end{aligned} \tag{2.32}$$

We should note that in Eq. (2.31) the first term has no dependence of the medium, this is the term that has to be regularized as the other terms become finite and do not need regularization. Furthermore, if we take the limit $T = \mu \to 0$ then $n_p = \bar{n}_p = 0$ and we recover the vacuum gap equation Eq. (2.8).

Next, we would like to add the medium to a proper time regularized gap equation. We start once again from Eq. (2.6). Then, we perform the same thermal substitutions as before and use the relation Eq. (2.9). This yields

$$\mathrm{i}\,\mathrm{I}(m) = T \sum_{n=-\infty}^{\infty} \int_0^\infty ds \int \frac{d^3k}{(2\pi)^3} e^{-(\omega_n^2+m^2)s}. \tag{2.33}$$

For our purposes, in the last equation we drop the chemical potential $\mu \to 0$. Thus, $\omega_n = (2\pi+1)\pi T$. Now, performing the momentum integrals in Eq. (2.33) drops a $\left(\sqrt{\frac{\pi}{s}}\right)^3$ term. Hence,

$$\mathrm{i}\,\mathrm{I}(m) = \int_{\Lambda_{PT}}^\infty ds \left(\frac{\pi}{s}\right)^{3/2} e^{-m^2 s} T \sum_{n=-\infty}^{\infty} e^{-\omega_n^2 s}, \tag{2.34}$$

where the infrared cutoff was added. We can identify the sum in the integral with the Jacobi $\Theta_2(z,\tau)$ function, defined as

$$\Theta_2\left(z,\tau\right) = \sum_{m=-\infty}^{\infty} e^{i\pi\tau(m+1/2)^2} e^{iz(2m+1)}. \tag{2.35}$$

Then, we have that

$$\Theta_2\left(i\,4\pi T^2 s, 0\right) \;\; = \;\; \sum_{n=-\infty}^{\infty} e^{-\left[2(n+1/2)\pi T\right]^2 s}. \tag{2.36}$$

Finally, using the inversion formula and the relationship between the Jacobi theta functions [16]

$$\Theta_2\left(i4\pi T^2 s, 0\right) = \left(4\pi T^2 s\right)^{-1/2} \Theta_3\left(\frac{i}{4\pi T^2 s}, \frac{\pi}{2}\right), \tag{2.37}$$

the integral $iI(m)$ can be written in the form

$$iI(m) = \frac{\pi^{3/2}}{\left(4\pi\right)^{1/2}} \int_{\Lambda_{PT}}^{\infty} ds\, \frac{1}{s^2} e^{-m^2}\, \Theta_3\left(\frac{i}{4\pi T^2 s}, \frac{\pi}{2}\right), \tag{2.38}$$

where

$$\Theta_3\left(\frac{i}{4\pi T^2 s}, \frac{\pi}{2}\right) = 1 + 2\sum_{n=1}^{\infty} \left(-1\right)^n e^{-\frac{n^2}{4T^2 s}}. \tag{2.39}$$

After this process, the gap equation takes the form

$$m = m_q + \frac{3}{\pi^2} G\, m \int_{\Lambda_{PT}}^{\infty} \frac{ds}{s^2}\, e^{-m^2 s}\, \Theta_3\left(\frac{i}{4\pi T^2 s}, \frac{\pi}{2}\right). \tag{2.40}$$

In the next Chapter we use the gap equations calculated here to sketch the NJL phase-diagram using the Lagrange multipliers method.

# THE CRITICAL CONDITION

# 3

# THE PHASE DIAGRAM OF THE NJL MODEL

It is widely accepted that after the Big Bang, the universe was so hot and dense that underwent several phase transitions. Just between $10^{-12}$ and $10^{-5}$ seconds after the Big Bang, the universe was cold enough that it was possible to differentiate the strong from the electroweak interactions but still too hot to form hadrons. Instead, the quarks transitioned into a phase known as the Quark-Gluon-Plasma (QGP). Some time later, the temperature decreased enough and the quarks underwent another phase transition and bind into hadrons. These early universe temperature and density conditions are met in relativistic heavy-ion collisions experiments as the ones carried out at RHIC [17] and the LHC [18] to explore the phase diagram of QCD. In Fig. 3.1 we can see the conjectured phase-diagram of QCD. Over the time, several methods have been used to study the QCD phase diagram such as LatticeQCD [19, 20], Schwinger-Dyson equations [21], effective models such as the sigma model [22], Functional Renormalization Group methods [23] among others. On one hand, these approaches have found that at vanishing chemical potential, a crossover occurs at $T_c \approx 170 - 186$ MeV for 2 light quark flavors [24, 25] and around $T_c \approx 150 - 156.5\,\text{MeV}$ [26, 27] when the strange quark is added into the mix. In the chiral limit, the transition becomes of second order. On the other hand, various effective model have found that at zero temperature and large chemical potential $\mu$, the transition is of first order. These two facts hint toward the existence of the Critical End Point (CEP), at which the two aforementioned transitions meet.

Current and planned experiments at FAIR [28, 29], RHIC [30] , LHC [31] and NICA [32] hope to create QGP and explore the QCD phase diagram by colliding heavy-ion at ultra-relativistic velocities. Fig. 3.2 shows a schematics of the collision of heavy-ions, in this picture the squashed ions gets closer to each other in a) and b) then they pass each other in c) where the collision is capable of producing enough temperature and density to potentially create QGP. In this phase of the collision, the QGP behaves like an almost perfect fluid [33, 34]. Finally, the system expands, cools down and

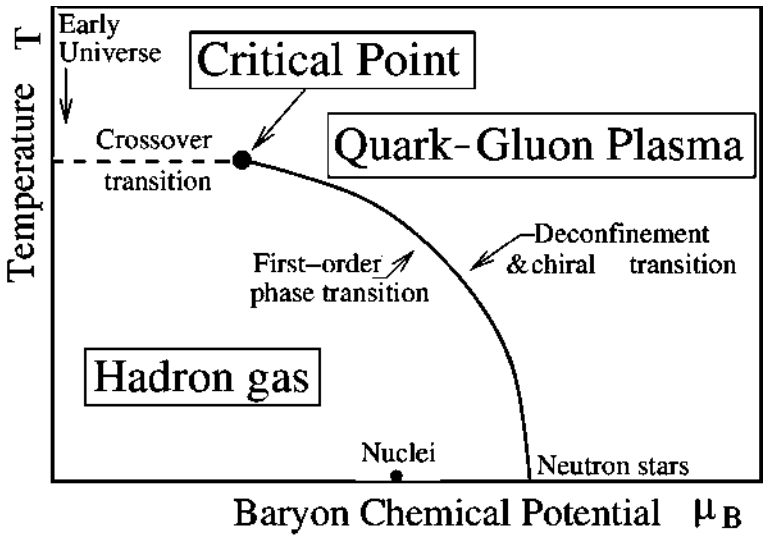


Figure 3.1: Sketch of the QCD phase-diagram.

hadronizes d). This heavy ion collision can be modeled in multiple stages taking into account each epoch of the collision [35].

## 3.1 THE PHASE-DIAGRAM OF THE NJL MODEL

As expected, in the NJL model the phase diagram is sightly different from the phase diagram of full QCD. There have been several attempts of describing the properties of the QCD phase diagram employing the NJL model [6, 36, 37], coupling it to a Polyakov loop potential [4, 38], adding a medium dependent coupling [39–43], non-local extensions [44] among others. The fact that it is not renormalizable means the location of the phase boundaries depends on the fitting of the regularization parameter $\Lambda$ as described in Chapter 1.

These boundaries are defined by the behavior of the order parameter, the quark condensate $\langle\bar{\psi}\psi\rangle$, as a function of the thermodynamic parameters, temperature $T$ and chemical potential $\mu$; for a second order phase transition, the change in the order parameter is continuous whereas for a first order phase transition, the order parameter evolves discontinuously. In the crossover the variation of the quark condensate is

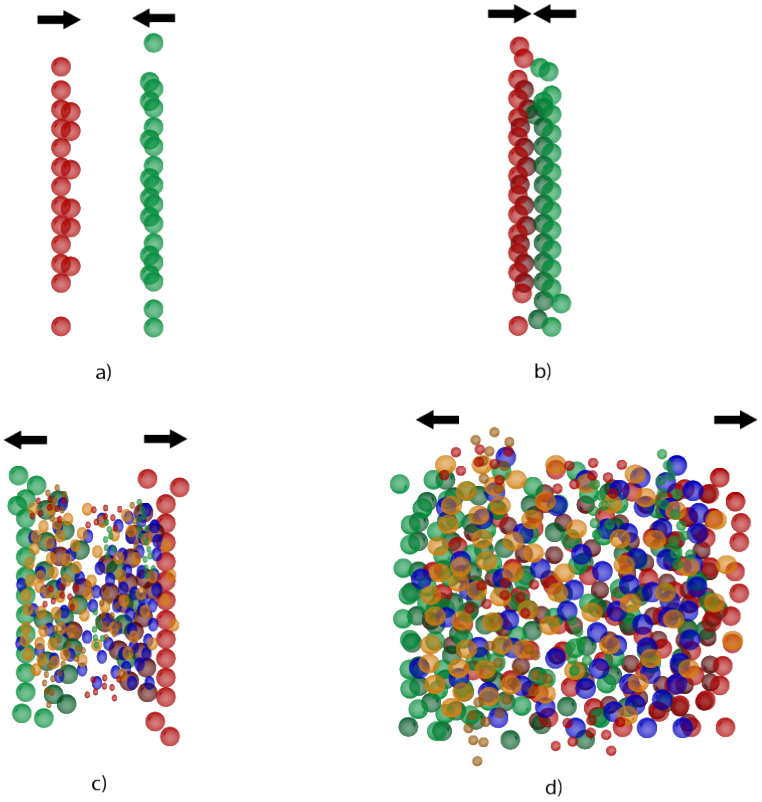


Figure 3.2: Schematics of heavy ion-collision. In this picture the squashed ions gets closer to each other in a) and b) then they pass each other in c). Finally, the system expands, cools down and hadronizes d).

smooth but it changes sufficiently fast that it can be defined as the maximum of the chiral susceptibility. Given that in the NJL model the chiral condensate $\langle\bar{\psi}\psi\rangle$ is proportional to the dynamically generated mass $m$, any change in the chiral condensate is reflected in the dynamical mass. Therefore by exploring the dynamical mass generation phenomenon, we explore the phase diagram.

## 3.2 THERMODYNAMIC POTENTIAL

In practice, there are various ways to obtain the phase boundaries. One has to do with the thermodynamic potential, defined as:

$$\Omega(T,\mu) = -\frac{T}{V}\ln\mathcal{L} = -\frac{T}{V}\ln \mathbf{Tr}\exp\left(-\frac{1}{T}\int d^3x\left(\mathcal{H}-\mu q^\dagger q\right)\right), \tag{3.1}$$

where $\mathcal{H}$ is the Hamiltonian density, **Tr** a functional trace over all state of the system and $\mathcal{L}$ is the grand canonical partition function. As usual, from Eq. (3.1) one can get all the thermodynamic quantities from the system. In the NJL model, the thermodynamic potential takes the form [6]:

$$\begin{aligned}\Omega(T,\mu;m,m_q) &= -2N_fN_c\int\frac{d^3k}{(2\pi)^3}\left\{E_k + T\ln\left(1+\exp\left[-\frac{E_k-\mu}{T}\right]\right)\right.\\ &+ \left. T\ln\left(1+\exp\left[-\frac{E_k+\mu}{T}\right]\right)\right\} + \frac{(m-m_q)^2}{2G}.\end{aligned} \tag{3.2}$$

Here $m$ is the dynamical mass, $m_q$ the current quark mass and $G$ is the coupling constant. The way to get the transition boundaries relies in obtaining the minima of the thermodynamic potential with respect of the mass; a second order transition is characterized by a curve in which besides the minimum corresponding to the trivial mass solution $m = 0$ a second minimum begins to develop corresponding to a non trivial solution of the mass $m \neq 0$. This minimum splits from the minimum belonging to the trivial one in a smooth way, as can be seen in Fig. 3.3; here, schematically, for low values of temperature, in this example for $T = 0.01$ GeV and $\mu = 0$, the minimum correspond to a zero value of the dynamical mass and chiral symmetry is broken (upper panel). As the temperature raises, the minimum moves towards $m = 0$. As the transition is smooth, this displacement is smooth too.

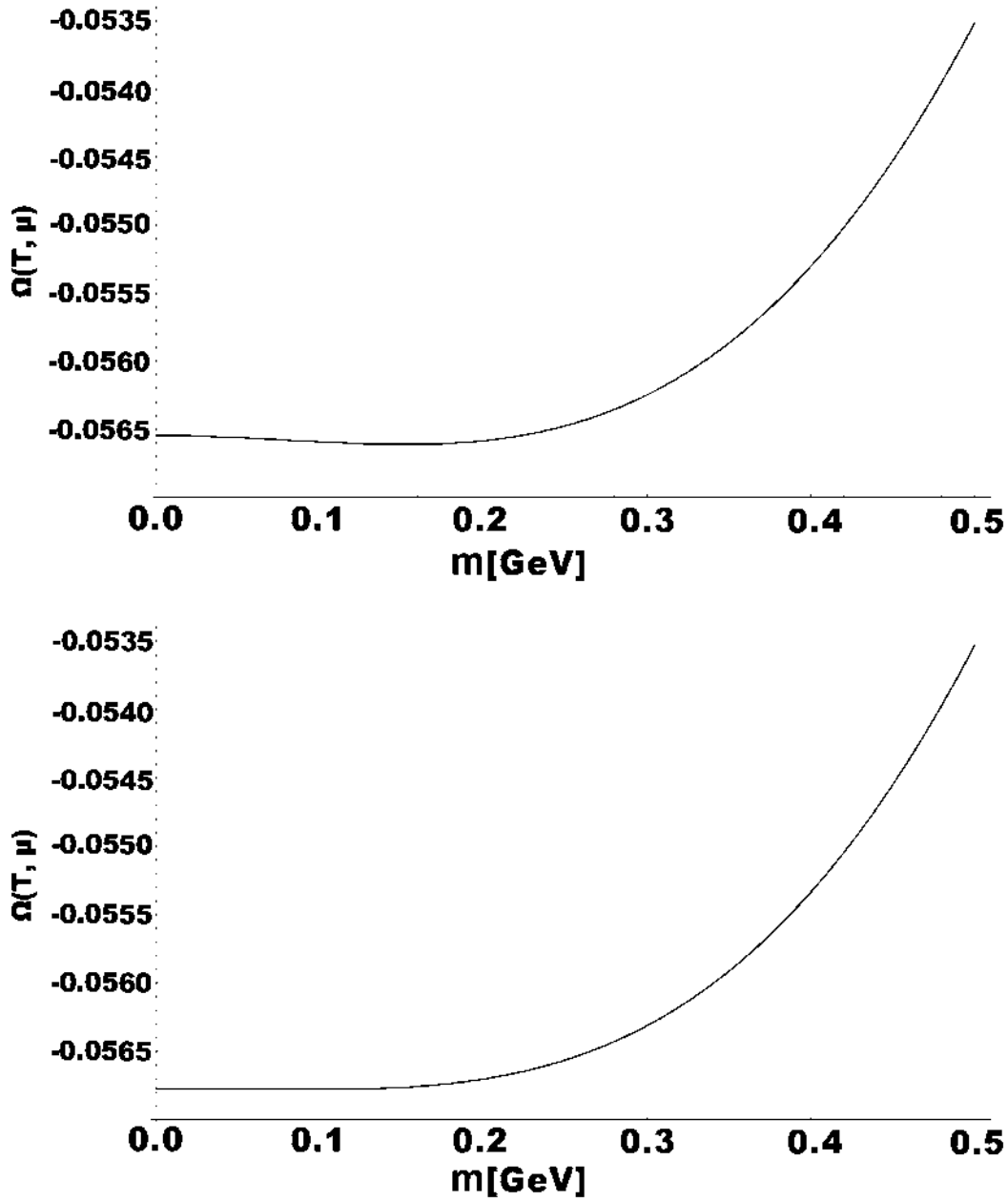


3.3

Figure 3.3: Determination of a second order phase boundary using the thermodynamic potential. Note how the minimum moves to the $m = 0$ axis.

On the other hand, in Fig. 3.4 we can see what happens to the thermodynamic potential that undergoes a first phase transition. As in the second order transitions, here the thermodynamic potential also develops a minimum at $m \neq 0$ (upper panel) and a maximum located at $m = 0$ for $\mu = 0$ and $T = 0.001$ GeV. As the chemical potential increases, the minimum begins to move but as the chemical potential reaches a critical value $\mu_p \approx 0.3$ GeV, the minimum jumps and settles at $m = 0$ (lower panel). These jumps is what characterizes a first order phase transition.

It is easy to see that the next step to obtain the phase diagram boundaries is to get the minima of the thermodynamic potential. It turns out that this minimum corresponds to the gap equation obtained in Chapter 1.

## 3.3 THE GAP EQUATION FROM THERMODYNAMIC POTENTIAL

As we said earlier, when we minimize the thermodynamic potential the resulting relation is the gap equation. Explicitly, it is easy to see that

$$\frac{\partial \Omega}{\partial m} = 0 = \frac{m - m_q}{2G} - 2N_f N_c \int \frac{d^3k}{(2\pi)^3} \frac{m}{E_k} \left(1 - n_k(T,\mu) - \bar{n}_k(T,\mu)\right). \tag{3.3}$$

We can see that the resulting equation is the same as the gap equation in Eq. (2.31). In principle, the gap equation is enough to find the phase boundaries; the development of non-trivial minima in the thermodynamic potential for a set of fixed values means that the gap equation has a non trivial solution for the mass, $m \neq 0$, and although the method seems straightforward, in practice this implies that we need to solve the gap equation for every set of parameters $(T, \mu; G, \Lambda)$ to check if the chiral symmetry is broken or not. We can then draw the phase diagram with all the values obtained.

## 3.4 CRITICAL COUPLING IN VACUUM

Out next goal is to introduce another method to draw the phase diagram but first we need to check the solutions to the gap equation. In Fig. 3.5 we can see an example of the solution of the gap equation, Eq(3.3), as a function of the coupling constant $G$ for various values of the temperature $T$ and fixed chemical potential $\mu = 0$. As

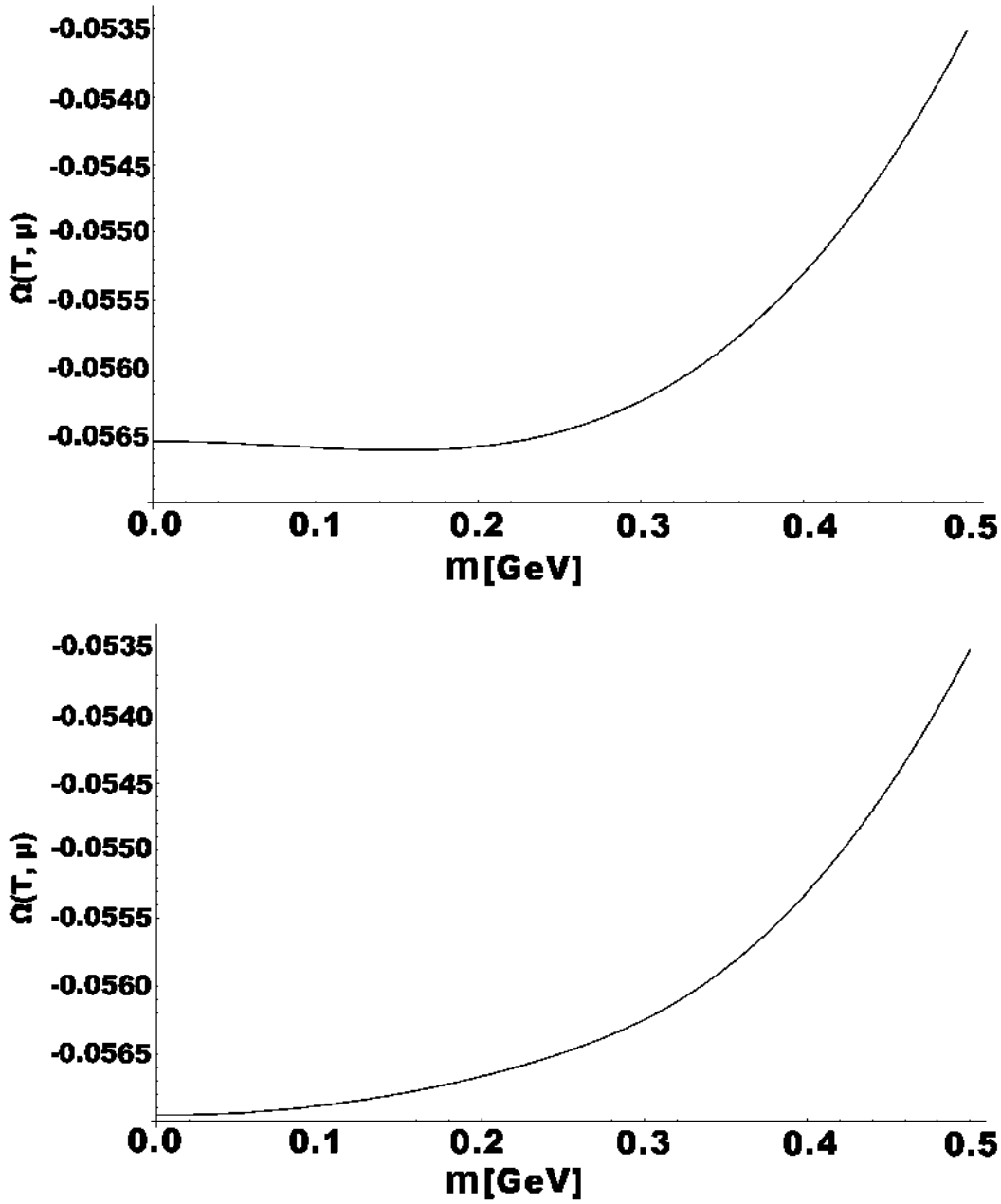


Figure 3.4: Determination of a first order phase boundary using the thermodynamic potential. Note how the minimum moves toward the $m = 0$ axis.

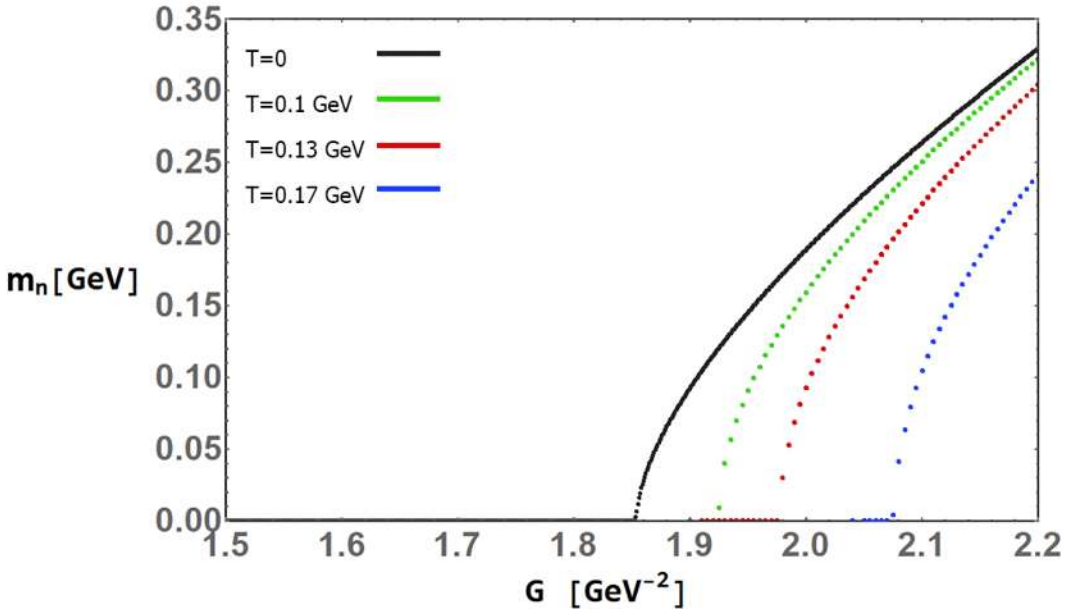


Figure 3.5: Plot of the solutions of Eq. (3.3) as a function of the coupling constant. It is easy to see that the coupling strength needed to trigger the formation of the chiral condensate increases as temperature raises. The equation was solved iteratively as described in [10]. $\mu = 0$ for all cases.

can be seen, the coupling strength necessary to trigger the dynamical generation of mass, the critical coupling. $G_c$, increases as temperature increases. This is a very well known fact, as the effect of the thermal bath is to inhibit the formation of the chiral condensate. We can actually get the value of the critical coupling, but first we need to consider the right and left hand side of the gap equation independently. Starting with the gap equation in vacuum, Eq. (2.8), we define:

$$\begin{aligned} y &= m, \\ F(m) &= m\,\frac{NN_c}{\pi^2}\left\{\Lambda\sqrt{\Lambda^2+m^2} - m^2\ln\left(\frac{\Lambda+\sqrt{\Lambda^2+m^2}}{m}\right)\right\}. \end{aligned} \tag{3.4}$$

In Fig. 3.6 we see the plots of the left hand side and right hand side of the gap equation, Eq. (2.8), as a function of the dynamical mass $m$. At $G = 1.5$ GeV$^{-2}$, the coupling strength is not enough to break chiral symmetry and generate mass (upper

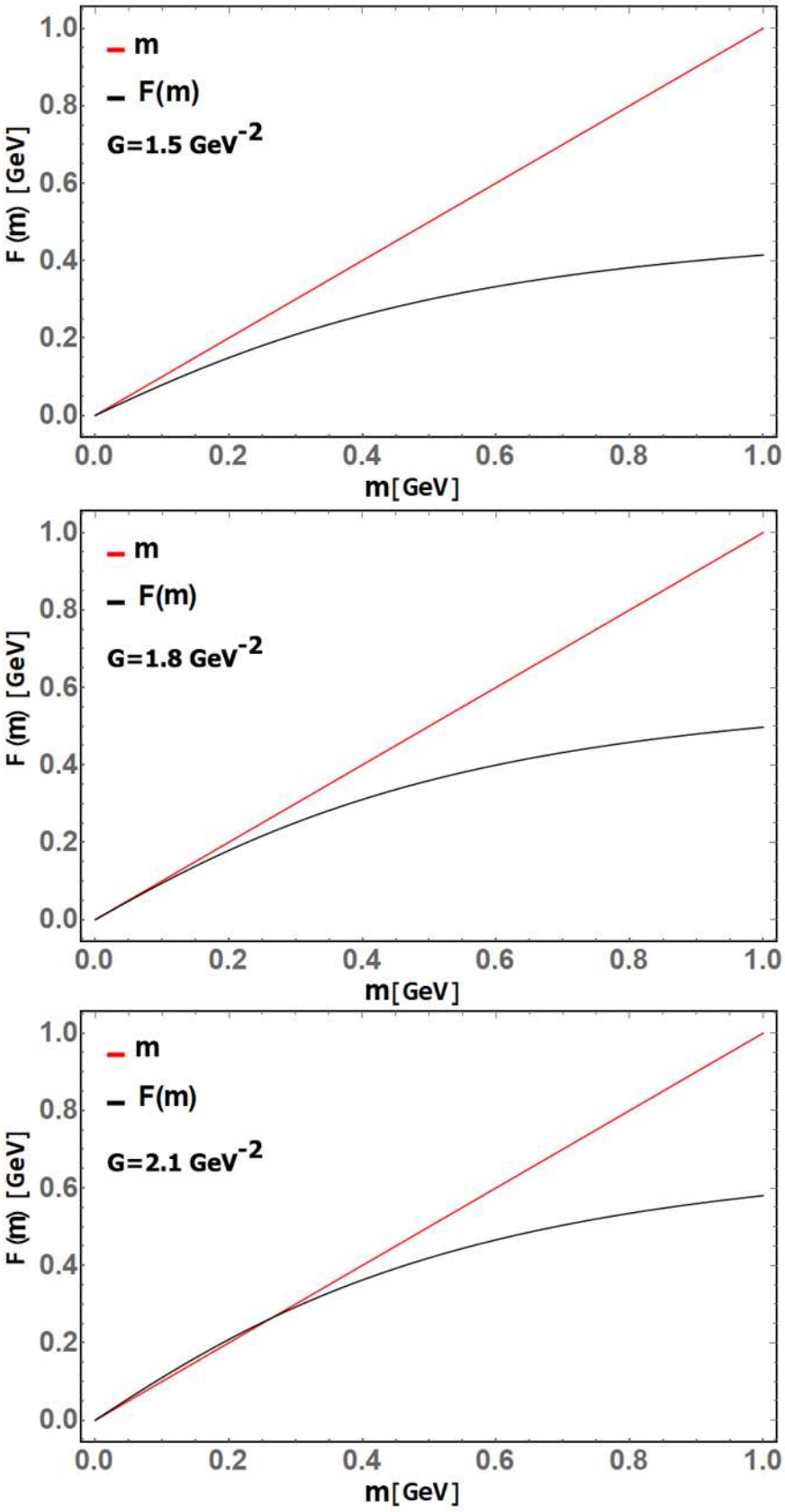


Figure 3.6: Plot of the right hand side and left hand side of the gap equation, Eq. (3.4), for various values of the coupling constant.

panel). As the coupling raises, $G = 1.8\ \text{GeV}^{-2}$, the two curves become tangent and the gap equation begins to develop non trivial solutions for the mass. This conditions characterize, the critical coupling $G_c$ (mid panel). Finally, for $G = 2.1\ \text{GeV}^{-2}$, the two curves intersect each other. At this point, the gap equation has stable non trivial solutions for the mass $m \approx 0.27\,\text{GeV}$.

Given the last example we can conclude that for the critical coupling, the following conditions holds

$$\frac{d}{dm}y = G_c \frac{d}{dm}F(m), \tag{3.5}$$

with the coupling constant acting as a control parameter. For Eq. (2.8), this condition yields:

$$1 = \frac{N_f N_c}{\pi^2} G_c \left[ \frac{\Lambda^3 + 3\Lambda m^2 - 3m^2\sqrt{\Lambda^2 + m^2}\,\ln\left(\frac{\Lambda+\sqrt{\Lambda^2+m^2}}{m}\right)}{\sqrt{\Lambda^2 + m^2}} \right]. \tag{3.6}$$

As the two curves in Fig. 3.6 become tangent at $m = 0$, the condition for the critical coupling in vacuum finally reads:

$$G_c = \frac{\pi^2}{6\Lambda^2} \approx 1.853\ \text{GeV}^{-2}. \tag{3.7}$$

Expectedly, the only dependence of the critical coupling is on the regulator $\Lambda$.

## 3.5 CRITICAL COUPLING IN A THERMAL BATH

Now we address the issue of getting the critical coupling in a thermal bath. The procedure is similar as in the previous Section. Once again, we define

$$\begin{aligned} y &= m, \\ F(m,T) &= 4N_f N_c\, m \int \frac{d^3k}{(2\pi)^3}\frac{1}{E_k}\left(1 - 2\frac{1}{e^{\frac{E_k}{T}}+1}\right), \end{aligned} \tag{3.8}$$

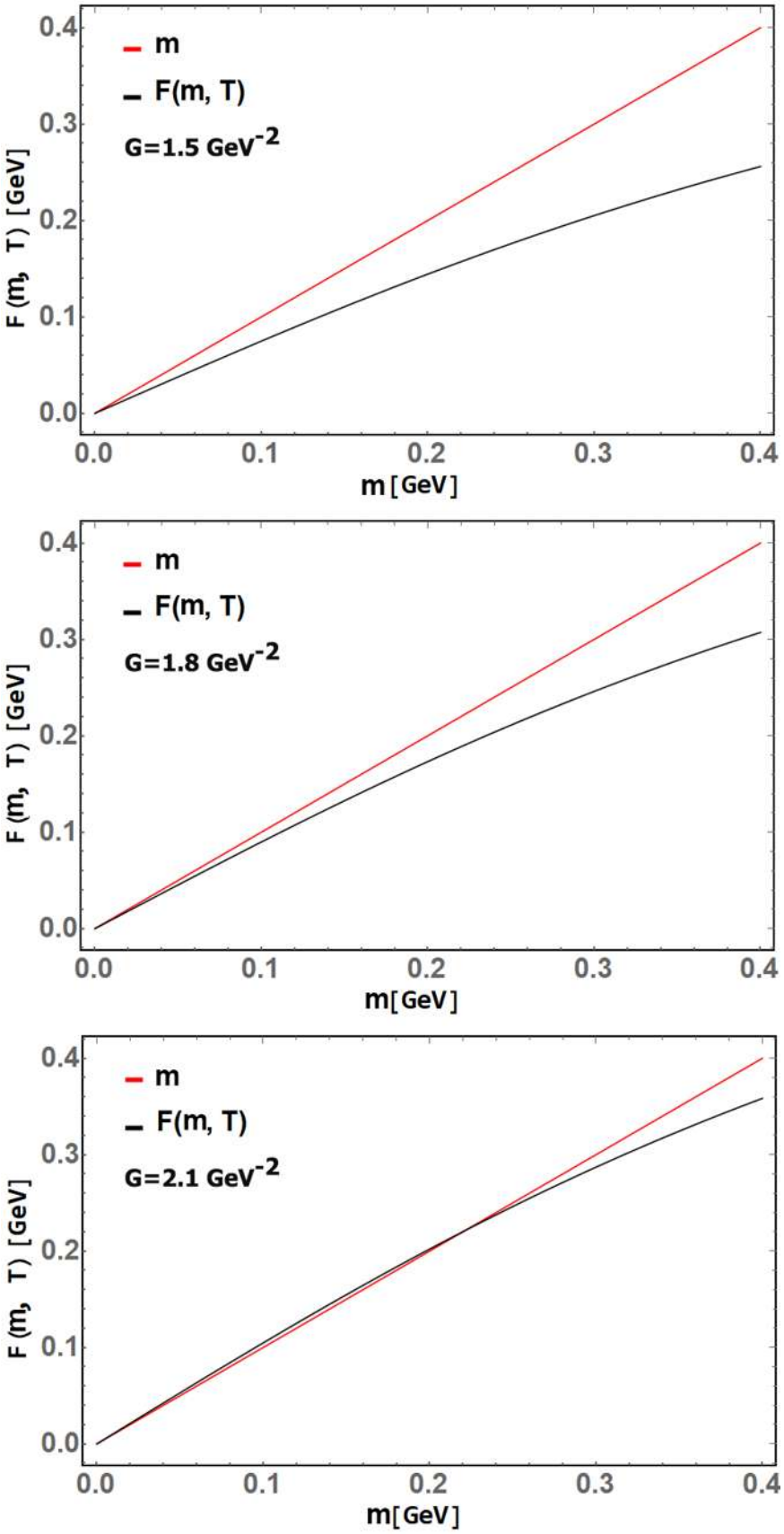


Figure 3.7: Plot of the right hand side and left hand side of the gap equation, Eq,. (3.8), for various values of the coupling constant. $T = 0.13$ GeV in all plots.

and proceed to plot. Fig. 3.7 is mostly similar to the vacuum case, the main difference is the effect of the temperature that, although small, is manifest in the need of a larger coupling to trigger the crossing of the plots. Proceeding similarly as before, we apply the condition defined in Eq. (3.5) and after we evaluate at $m = 0$, we get

$$1 = 4N_f N_c G_c \left[ \int_0^{\Lambda} \frac{dk}{(2\pi)^3} k - 2 \int_0^{\infty} \frac{dk}{(2\pi)^3} \left( \frac{k}{e^{\frac{k}{T}} + 1} \right) \right]. \tag{3.9}$$

Note that the last integral on the above expression is not regularized. This because the vacuum and thermal contribution of the gap equation split. Physically, the thermalized plasma doesn't get affected by the vacuum divergencies and thus the thermal contribution is finite. Then, after performing the integrals, the critical coupling is

$$G_c = \frac{\pi^2}{2} \left( \frac{1}{3\Lambda^2 - \pi^2 T^2} \right). \tag{3.10}$$

In Fig. 3.8 we shown the plot of Eq. (3.9). The black curve is the boundary that divides the broken from the unbroken phases. As expected, the coupling needed to break chiral symmetry raises as the temperature increases. Furthermore, there exists a limiting temperature $T_L = \sqrt{\frac{3\Lambda^2}{\pi^2}}$ where $G_c$ diverges, which means that no matter how strong the coupling is, it is not enough to break chiral symmetry. For our input values, $T_L \approx 0.519$ GeV.

## 3.6 CRITICAL COUPLING IN A HOT AND DENSE MEDIUM

We leave the discussion of the critical coupling for later as the inclusion of the chemical potential needs special considerations. As before, we start by plotting the left and right hand side of the gap equation, Eq. (2.31), in the chiral limit $m_q \to 0$. We define:

$$\begin{aligned} y &= m, \\ F(m, T, \mu) &= 4N_f N_c G\, m \int \frac{d^3k}{(2\pi)^3} \frac{1}{E_k} \left(1 - n_k(T, \mu) - \bar{n}_k(T, \mu)\right). \end{aligned} \tag{3.11}$$

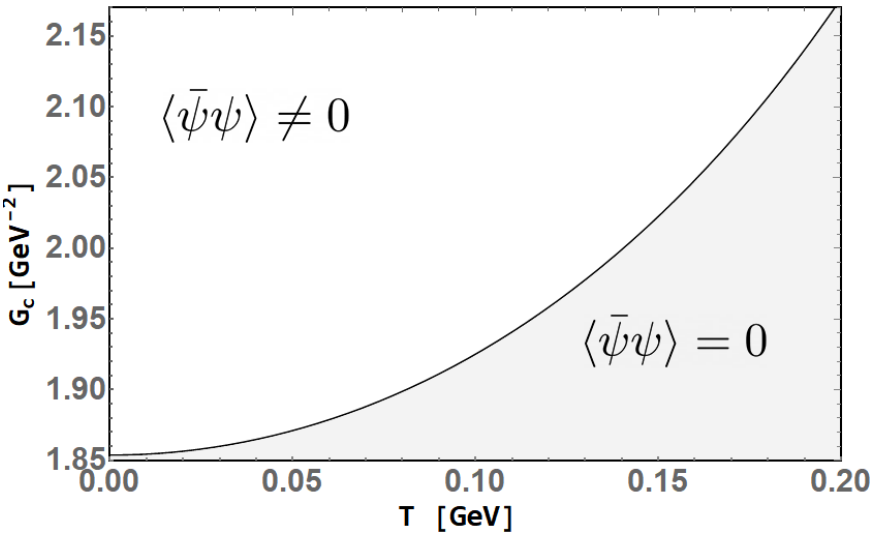


Figure 3.8: Critical coupling of the NJL model on a thermal bath. The regularization parameter $\Lambda = 0.942$ GeV.

Fig. 3.9 shows that the effect of the chemical potential is to form a concavity on the curve Eq.(3.11). In a), the coupling is not strong enough to break the symmetry, $G = 2.0$ GeV$^{-2}$, and as the coupling increases to $G = 2.55$ GeV$^{-2}$ in b) the two curves begin to cross each other but unlike in the previous cases, here there is a jump in the generated mass. This is a signal of a first order phase transition. As the coupling increases even further and reaches a value of $G = 2.65$ GeV$^{-2}$, in c) we notice that two curves cross each other in two points, meaning that the gap equation has developed two non trivial solutions. It should be stressed, nonetheless, that even though two solutions of the gap equation exists, only the largest minimizes the thermodynamic potential and furthermore, the largest solution is the stable one. At $G = 3.0$ GeV$^{-2}$ only the largest solution remains, whereas the other solution become zero.

This scenario calls for a modification of the method we have been using to obtain the critical condition, that is, apply Eq. (3.5), then evaluate the resulting expression at $m = 0$. This is no longer correct as the two curves can be tangent on $m = 0$ or $m \neq 0$, depending on the temperature and chemical potential. To solve this issue, we use Lagrange Multipliers.

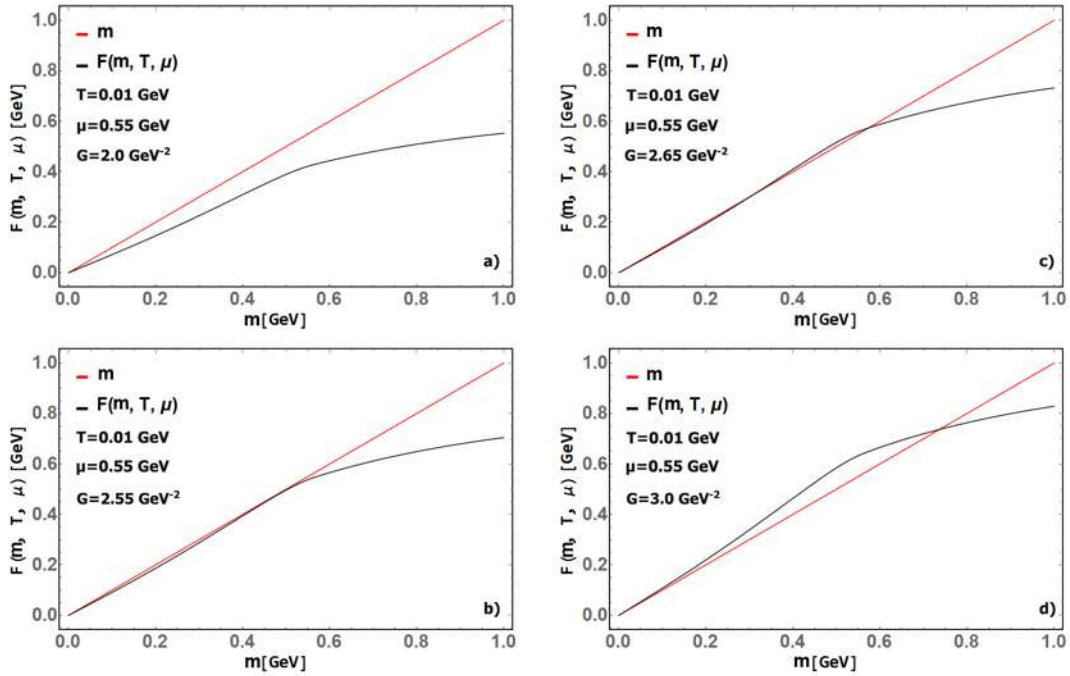


after

Figure 3.9: Plot of Eqs. (3.11) for various values of the coupling. The inclusion of the chemical potential makes the black curve to develop a concavity.

## 3.7 LAGRANGE MULTIPLIERS AND THE GAP EQUATION

The inclusion of Lagrange Multipliers is natural when we talk about maximizing any curve subject to a constraint. In our quest to obtain the critical coupling of the gap equation, we include the Lagrange Multipliers method as follows:

- The curve $F(m, T, \mu, ...)$ is the function to maximize.
- $y = m$ becomes the constraint.
- The coupling constant $G$ acts as the Lagrange multiplier we want to know.

In this framework, the conditions to find for the critical coupling are

$$m = G_c F(m, T, \mu, ...; \Lambda), \tag{3.12}$$

$$\frac{d}{dm} y = G_c \frac{d}{dm} F(m, T, \mu, ...; \Lambda). \tag{3.13}$$

Redefining $F(m, T, \mu, ...; \Lambda) = m\, H(m, T, \mu, ...; \Lambda)$, we can write Eq. (3.13) as

$$1 = G_c \left[ H(m, T, \mu, ...; \Lambda) + m \frac{d}{dm} H(m, T, \mu, ...; \Lambda) \right]. \tag{3.14}$$

Multiplying by $m$ in both sides of the equation and using Eq. (3.12), we arrive at the **critical condition**

$$m^2 \frac{d}{dm} H(m, T, \mu, ...; \Lambda) = 0, \tag{3.15}$$

where $m$ is the dynamically generated mass. Notice the absence of the coupling constant. Now, Eq. (3.15) defines the combination of parameters that give raise to a phase transition, if the only solution available is the trivial one $m = 0$. Then, for that combination of parameters, the transition is of second order. If besides the trivial solution we can find a non trivial one, then for that set of parameters, the transition is of first order. The reason for this conclusion is that Eq. (3.15) encodes where Eq. (3.13) must be evaluated for the relation to be fulfilled and the coupling critical.

The steps to get the critical coupling from Eq. (3.15) are the following:

- Fix the value of the regularization parameter $\Lambda_0$. Then, choose starting values for the temperature and the chemical potential $T_0$, $\mu_0$, etc...
- Solve Eq. (3.15) and pick the maximum solution available (either trivial or non-trivial solution), $m_0$.
- The critical coupling for the chosen values of temperature and chemical potential can be obtained using Eq. (3.12) as

$$G_c = \frac{m_0}{F(m_0, T_0, \mu_0, ...; \Lambda_0)}.$$

## 3.8 FROM THE CRITICAL COUPLING TO THE PHASE-DIAGRAM

Even though we have obtained the critical coupling $G_c$ for the various types of phase transitions, our main interest is in sketching the phase-diagram of the NJL model. It turns out that, from the critical condition, we can draw the phase diagram. This is easy to see if we the plot the set of $(G_i, T_i, \mu_i)$ values obtained from the critical condition Eq. (3.15) as shown in Fig. 3.10; this plot displays all the values of the coupling from which a first (blue) or second (orange) order phase-transition occur. All this means that in order to get the phase diagram for a chosen value of the coupling, say $G_0$, all we have to do is slice the surface shown in Fig. 3.10 for the selected value of the coupling $G_0$.

We present use cases of this method in the next Chapter.

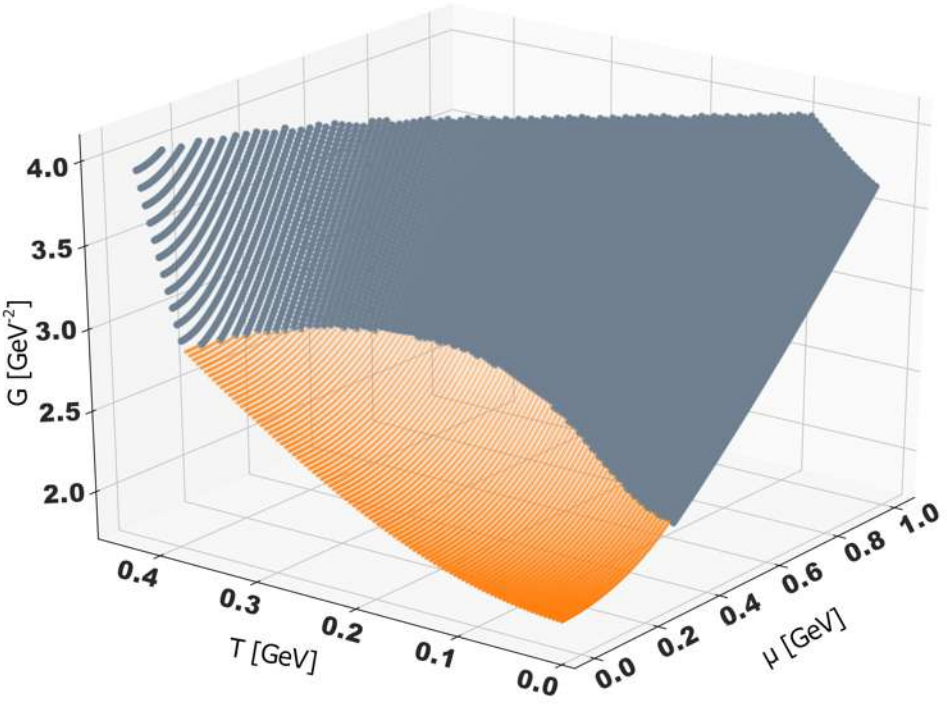


Figure 3.10: Plot of all the values $(G_i, T_i, \mu_i)$ obtained from the critical condition Eq. (3.15). The regularization parameter was fixed at $\Lambda = 0.942\,\text{GeV}$.

# USING THE CRITICAL CONDITION

# 4

# THE CRITICAL CONDITION IN ACTION

This Chapter is devoted to explore various aspects of the phase-diagram of the NJL model using the critical condition, Eq. (3.15), developed in the previous Chapter.

## 4.1 CRITICAL COUPLING: MAGNETIC AND THERMAL CONTRIBUTION

As magnetic fields take an important role in the description of phenomenons in all scales of energies from magnetic fields at the galactic level, compact stars to atomic and subatomic scales as in condensate matter and peripheral relativistic heavy ions collisions, to name a few[1]. In this Section we explore the critical coupling for the NJL model immerse in a thermal bath and an uniform, but of arbitrary strength magnetic field.

Considering a uniform magnetic field of strength $B$ aligned with the third spatial axis. The translationally invariant part of the quark propagator adopts its Schwinger representation [47]

$$\begin{aligned} S(k) &= -i\int_{\Lambda}^{\infty}\frac{ds}{\cos(q_f Bs)}e^{is\left(k_{\parallel}^2-k_{\perp}^2\frac{\tan(q_f Bs)}{q_f Bs}-m^2\right)} \\ &\quad\left\{(\cos(q_f Bs)+\gamma_1\gamma_2\sin(q_f Bs))(m+\not{k}_{\parallel})\right. \\ &\quad\left.-\frac{\not{k}_{\perp}}{\cos(q_f Bs)}\right\}, \end{aligned} \tag{4.1}$$

1 For a review on the magnetized QCD phase diagram see [45] and for a review of peripheral heavy ion collision magnetic fields, see [46].

where $q_f$ is the absolute value of the quark charge and $k_\parallel$ and $k_\perp$ are the parallel and perpendicular components of the four-momentum defined as

$$\begin{aligned} k_\perp^\mu &\equiv (0, k_1, k_2, 0), \\ k_\parallel^\mu &\equiv (k_0, 0, 0, k_3). \end{aligned}$$

. With Eq. (4.1), the gap equation in a thermal bath and a magnetic field takes the form

$$\begin{aligned} m &= m_q + GN_fN_c\frac{m}{2\pi^2}\left\{\int_\Lambda^\infty \frac{ds}{s^2}e^{-sm^2}\right. \\ &\quad + \int_0^\infty \frac{ds}{s^2}e^{-sm^2}\left(\frac{q_fBs}{\tanh(q_fBs)} - 1\right) \\ &\quad \left. + 2q_fB\int_0^\infty \frac{ds}{s}\frac{e^{-sm^2}}{\tanh(q_fBs)}\sum_1^\infty (-1)^n e^{-\frac{n^2}{4T^2s}}\right\}. \end{aligned} \tag{4.2}$$

The first integral in Eq. (4.2) is the vacuum term Eq. (2.12) and the second and third terms are the thermomagnetic contributions. These integrals converge as was the case with temperature and chemical potential. For comparison purposes, we take the limit $B \to 0$ and $m_q \to 0$. As the transition is of second order, then we use the critical condition, Eq. (3.13), to arrive at the critical coupling in a thermal bath for a proper time regularization,

$$G_c^T = \frac{\pi^2}{3}\Lambda\left(\frac{1}{1 - 2/3\Lambda\pi^2T^2}\right). \tag{4.3}$$

Fig. 4.1 shows the plot of the critical coupling, Eq. (4.3). Like the 3D cutoff critical coupling obtained before, Eq. (3.10), as the temperature raises, the coupling needed to break the symmetry gets larger. Furthermore, in this case, the limiting temperature at which the critical coupling $G_c^T$ diverges and is unable to break the chiral symmetry is $T_L^{PT} \approx 0.571$ GeV (with $\Lambda = 4.66 \times 10^{-1}$ GeV$^{-2}$, in accordance with Table 2.3) is comparable with the 3D cutoff regularization for which $T_L^{3D} \approx 0.519$ GeV.

Now, to find the influence of the magnetic field on the critical coupling, we set $T = 0$ on Eq. (4.2) and use the critical condition for the coupling, Eq. (3.13). We arrive at

$$1 = \frac{3}{\pi^2}G_c^M\left(\frac{1}{\Lambda} + \int_0^\infty ds\frac{1}{s^2}\left(\frac{q_fBs}{\tanh(q_fBs)} - 1\right)\right). \tag{4.4}$$

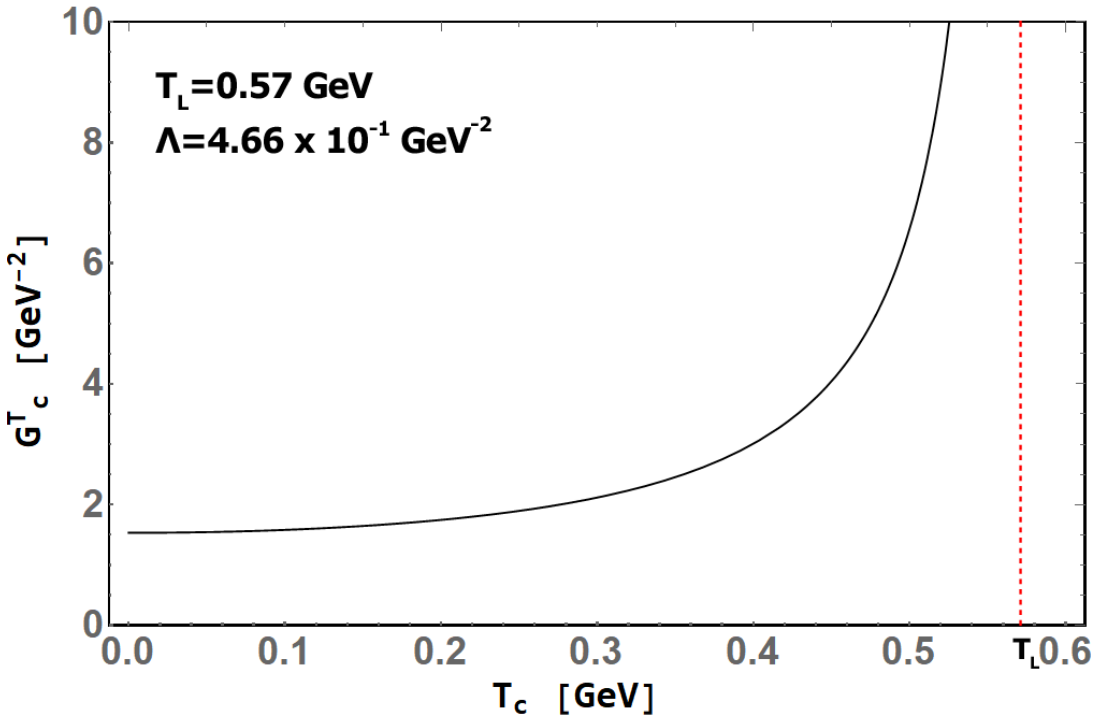


Figure 4.1: Critical coupling for the proper time regulated gap equation in a thermal bath. Notice the limiting temperature $T_L$.

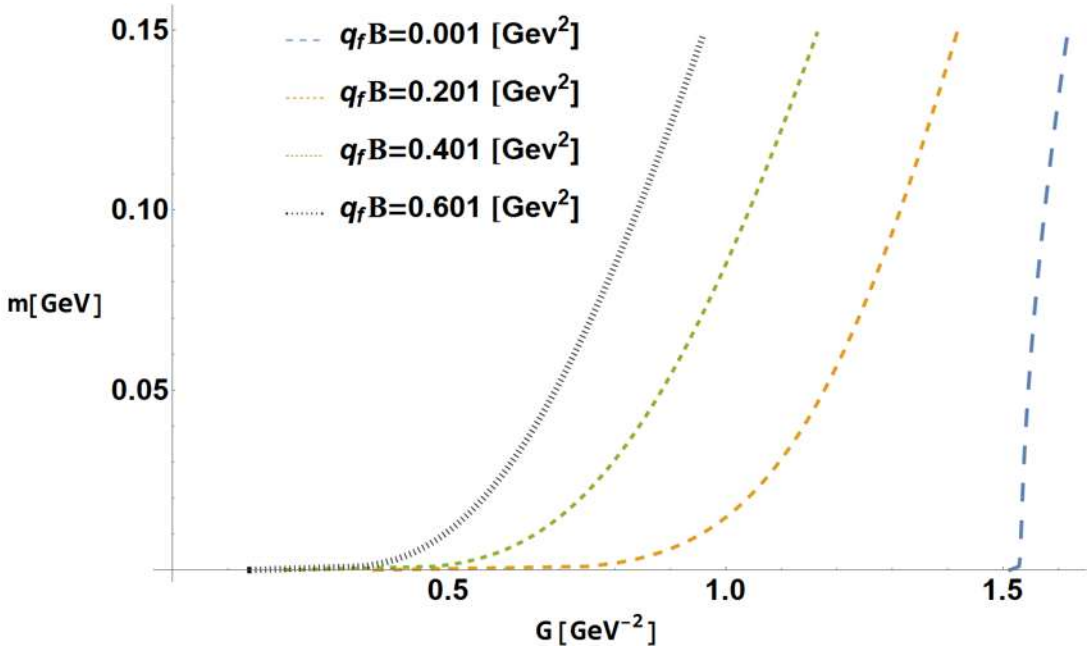


Figure 4.2: Plot of the mass function for the gap Eq. (4.2) with $T = 0$ for various values of the magnetic field. $\Lambda = 4.66 \times 10^{-1}$ GeV$^{-2}$. Notice the steep increase in the value of the mass.

Here we notice that the magnetic integral in Eq. (4.4) diverges. This means that the critical coupling is not defined. Therefore, for any non-zero value of the coupling, there is mass generation. This behavior is reminiscent of the magnetic catalysis phenomenon in which the magnetic field, at zero temperature, promotes the breaking of the chiral symmetry. An observation that can be done is that the generated mass is extremely small for small values of the coupling, Fig. (4.2). In this case, we can define a pseudo-critical coupling $\widetilde{G}_c^M$ defined as the coupling needed to generate a mass larger than the current quark mass, that is $m \sim \mathcal{O}(10^{-4}\,\text{GeV})$.

Fig. 4.3 shows the plot of the pseudo-critical coupling $\widetilde{G}_c^M$ as expected by the magnetic catalysis phenomenon the coupling needed to generate a set amount of mass drops as the magnetic field raises.

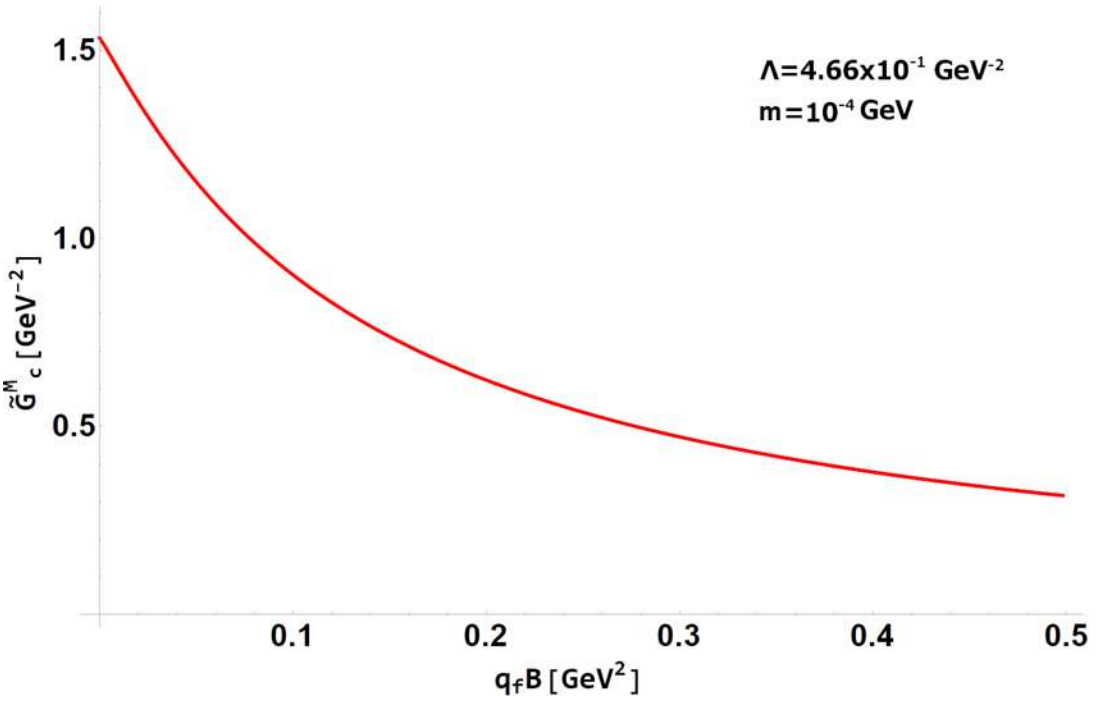


Figure 4.3: Plot of the pseudo-critical coupling defined as the coupling from which the generated mass exceeds $m \geq 10^{-4}\,\mathrm{GeV}$.

## 4.2 CRITICAL COUPLING: THERMO-MAGNETIC CONTRIBUTION

When we consider both the magnetic and thermal contributions the critical condition for the coupling reads

$$\begin{aligned} 1 &= \frac{3}{\pi^2} G^c_{MT} \left[ \frac{1}{\Lambda} + \int_0^\infty \frac{ds}{s^2} \left( \frac{q_f B s}{\tanh(q_f B s)} - 1 \right) \right. \\ &\left. + 2 q_f B \sum_{n=1}^{\infty} \int_0^\infty \frac{ds}{s} \frac{(-1)^n \exp(-s n^2)}{\tanh(\frac{q_f B}{4T^2 s})} \right], \end{aligned} \tag{4.5}$$

where once again, we have evaluated at $m = 0$ as the only transition possible is of second order. The effect that the magnetic field has on the critical coupling mainly is to greatly promote the breaking of the chiral symmetry even at very large values of the temperature, due the mechanism of magnetic catalysis, as can be seen in Fig. 4.4. Another trait that can be noticed is the delay in the appearance of the limiting temperature, from which the critical coupling diverges and is no longer capable of breaking the chiral symmetry, $T_L$, that moves towards larger temperatures.

## 4.3 CRITICAL COUPLING IN ARBITRARY DIMENSIONS

We can extend our ideas to an arbitrary number of dimensions $D$. The gap equation in vacuum takes the form

$$m = m_q + 2 D N_f N_c G \int_\Lambda \frac{ds}{(4\pi)^{\frac{D}{2}}} \frac{m}{s^{\frac{D}{2}}} e^{-s m^2}, \tag{4.6}$$

where $D$ is the number of dimensions in consideration. Before proceeding into applying the critical conditions, let us consider a variation of the proper time regularization, that adds an infrared cut off $\lambda$ with the aim of mimicking confinement by removing the poles of the propagator, [3, 48]

$$\begin{aligned} \int \frac{d^D k}{(2\pi)^D} \frac{1}{k^2 + m^2} &\rightarrow \int \frac{d^D k}{(2\pi)^D} \int_\Lambda^\lambda ds\, e^{-s\left(k^2 + m^2\right)} \\ &= \frac{1}{(4\pi)^{\frac{D}{2}}} \int_\Lambda^\lambda \frac{ds}{s^{D/2}} e^{-s\, m^2}. \end{aligned} \tag{4.7}$$

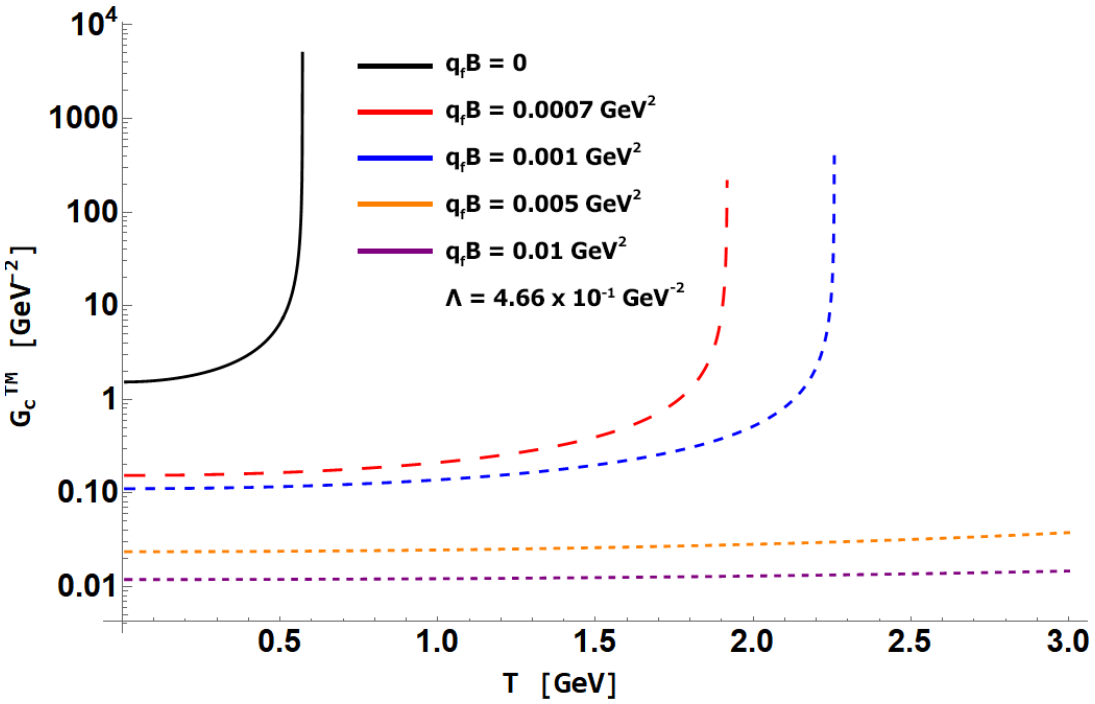


Figure 4.4: Critical coupling for the gap equation, Eq. (4.2), for various values of the magnetic field strength.

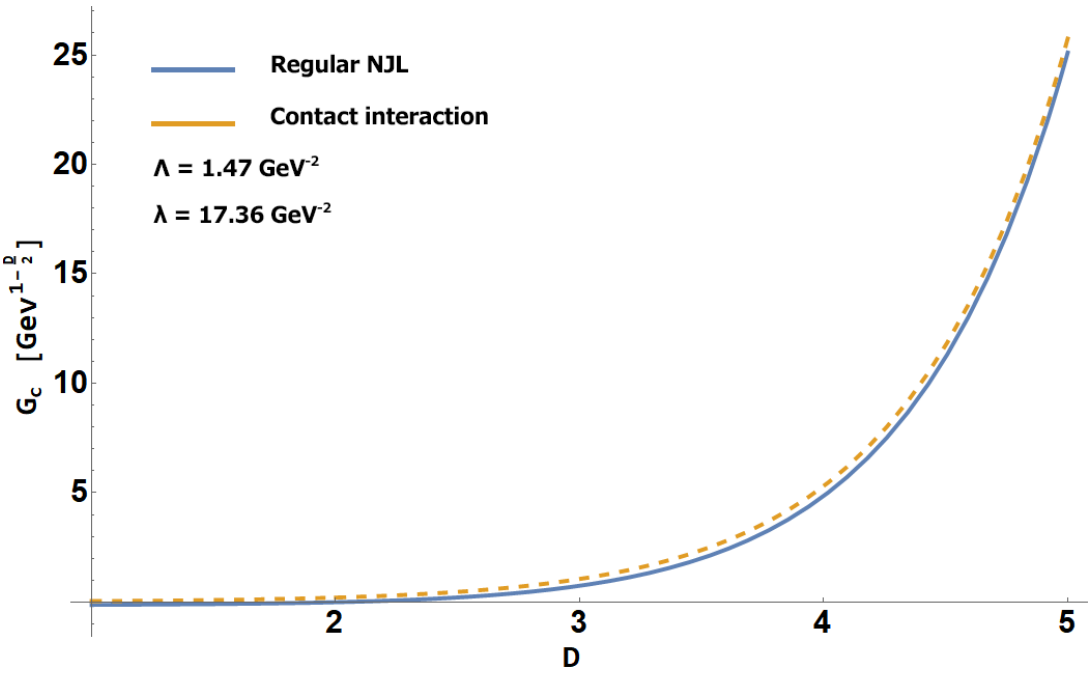


Figure 4.5: Plot of the critical coupling for the NJL model and the CI model as a function of the number of dimensions for the parameters shown in Table I in Ref. [3].

This regularization has been promoted in a symmetry preserving, Poincaré covariant vector-vector Contact Interaction (CI) model of QCD [49]. Using the critical condition, Eq. (3.13), yields

$$G_c^D = \frac{(4\pi)^{D/2}}{24\,D}\frac{(D-2)}{(\Lambda^{1-D/2}-\lambda^{1-D/2})}. \tag{4.8}$$

Fig. 4.5 shows the comparison of the NJL model and the CI model coupling as a function of the number of dimensions. As can be seen, as the number of dimensions increases, the required coupling to break the chiral symmetry increases. The case $D = 3$ is particularly interesting, given it mimics the dimensional reduction due an external magnetic field. Here we can see directly that indeed the case $D = 3$ requires a lower value of the coupling for both NJL and CI. In Fig. 4.6 we show the critical coupling as a function of the regularization parameter $\Lambda$ for the NJL model, note that for $D = 2$, the coupling necessary to break the chiral symmetry is zero for all values

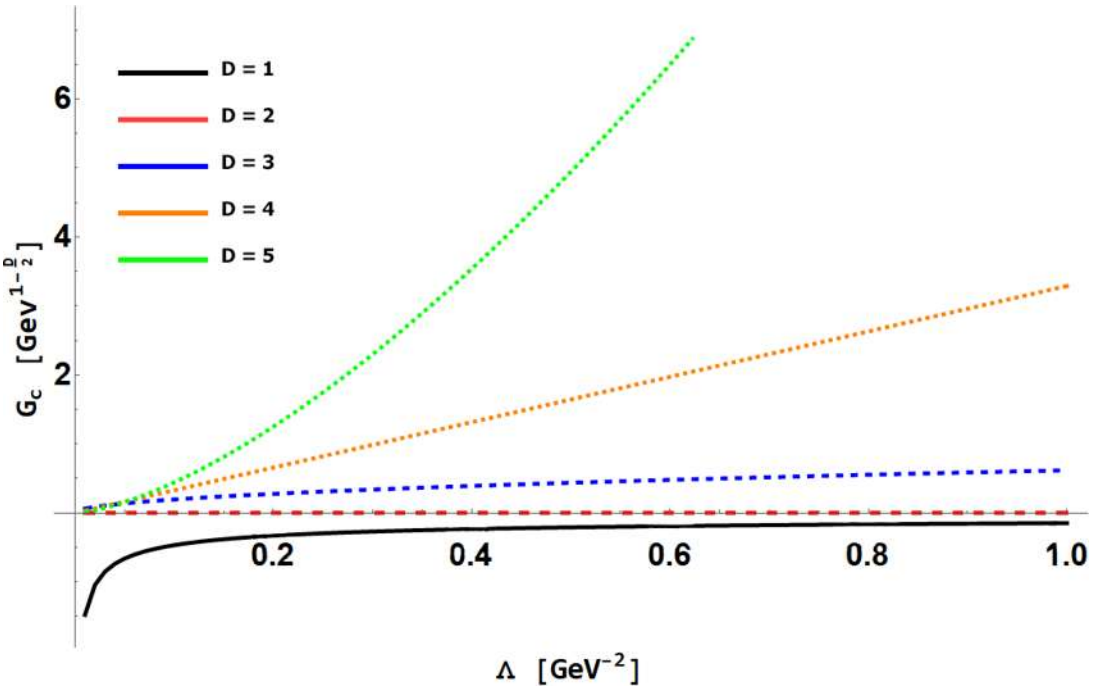


Figure 4.6: Comparison of the critical coupling for the NJL model in vacuum for various dimensions. Note that the necessary coupling in $D = 2$ is zero.

of $\Lambda$. Fig. 4.7 shows the same plot for the CI model. Unlike in the NJL model for $D = 2$, the critical coupling diverges for any value of the regularization parameters $\Lambda$ and $\lambda$.

## 4.4 THE PHASE DIAGRAM OF THE NJL MODEL

As was mentioned in Sec. 3.8, we can use the critical condition, Eq. (3.15), to draw the phase-diagram of the NJL model for any range of values of temperature $T$ and chemical potential $\mu$. To achieve this, let us consider the gap equation Eq. (2.31) and fix the regularization parameter $\Lambda = 0.942\,\text{GeV}$ . Plugging a range of values for the temperature and differentiating the values from which Eq. (3.15) yields zero and non-zero solutions for the mass, then plugging this values to get the corresponding coupling, we get to draw Fig. 4.8, where the orange area represents the space where

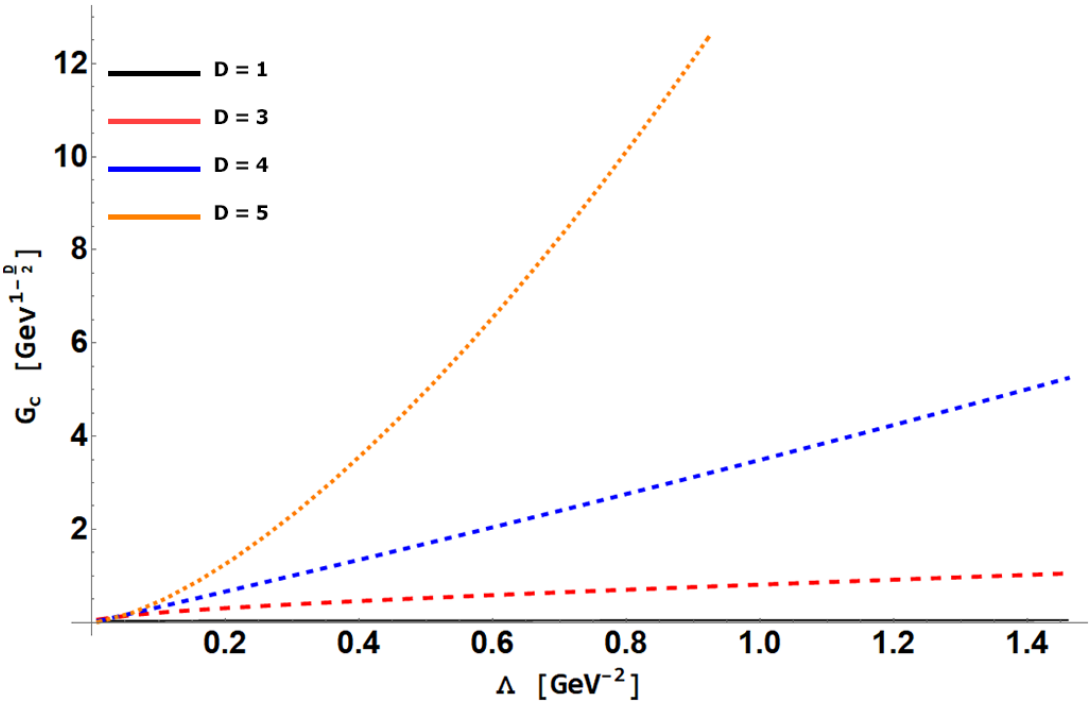


Figure 4.7: Comparison of the critical coupling for the CI model in vacuum for several dimensions.

only one solution $m = 0$ was found, whereas the blue area is where two solutions $m = 0$ and $m \neq 0$ where found.

To draw the actual phase diagram, we slice Fig. 4.8 in the desired value of the coupling. The sketch of the phase diagram can be seen in Fig. 4.9. For $G = 2.6$ GeV$^{-2}$ (upper panel), the phase diagram shows two main phases; in orange the area where the second order phase transition occurs, and the gray area, where the first order phase transitions occur. At this value of coupling, the critical chemical potential $\mu_c$ is located at $\mu_c \simeq 0.566\,\text{GeV}$, whereas the critical temperature is at $T_c \approx 0.321$ GeV and the location of the CEP is $T_{CEP} \approx 0.165$ GeV and $\mu_{CEP} \approx 0.423$ GeV. In the mid plot, $G = 3.0$ GeV$^{-2}$ and the phase diagram is very different from before. Here, the area corresponding with the first phase transition (gray) wraps around the second phase area (in orange). This situation results in a disconnection between the unbroken and the second order boundary and the disappearance of the CEP. Also, note the increase in the critical temperature $T_c \approx 0.4$ GeV and the critical chemical potential $\mu_c = 0.733$ GeV. Finally, in the third plot, $G = 3.5$ GeV$^{-2}$. Here, the wrapping is more noticeable, the separation of phases larger and the critical temperature and chemical potential increased once again with $T_c \approx 0.4717$ GeV and $\mu_c \approx 0.936$ GeV.

As we have seen, we were able to draw a phase diagram with some traits similar to the one found by LatticeQCD and other methods and models (upper panel of Fig. 4.9) but also we got some diagrams that do not resemble any other result before. One cause for that is that the values selected for the coupling are out of the scope of the model and therefore the result obtained. In this sense, care must be have in the parameters choice.

## 4.5 PHASE DIAGRAM - THE MEDIUM CONTRIBUTION

In Sec. 3.5 we mentioned that the medium contribution to the gap equation converges and thus the regularization was not necessary. In this Section we explore what is the effect of regularizing the medium contribution. The plot of the critical coupling can be seen in Fig. 4.10 and the phase diagram is drawn in Fig. 4.11. At first glance, we notice that the choice of regularizing the medium contribution avoids the wrapping of the first order phase transition area (in gray) around the second order phase transition area (in orange). For $G = 2$ GeV$^{-2}$ the CEP no longer exists as there is no first order phase transition taking place. $G = 3.0$ GeV$^{-2}$ is somewhat akin at what

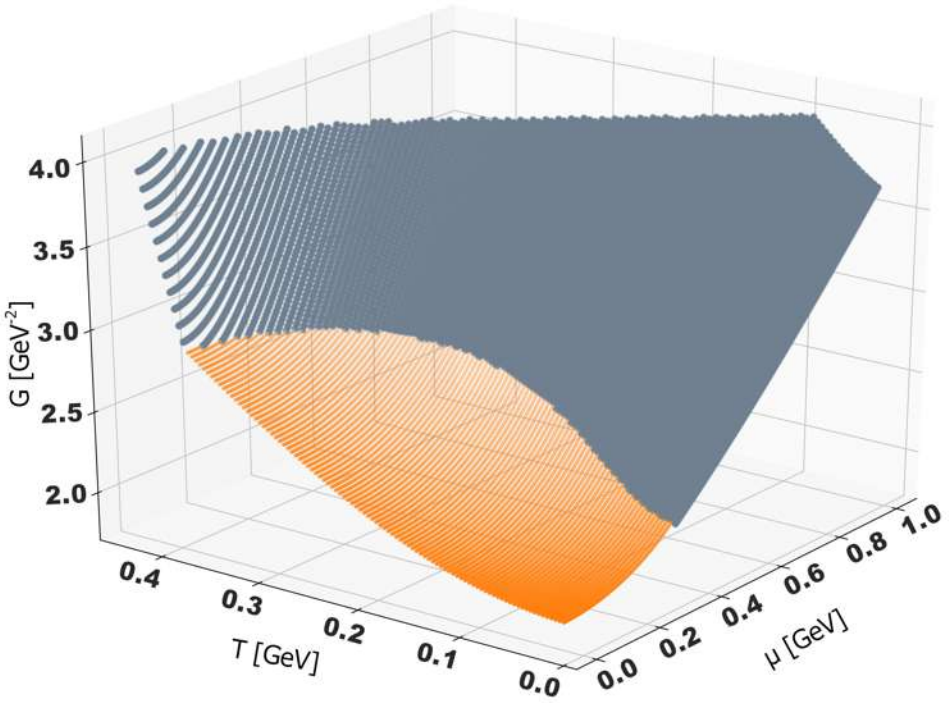


Figure 4.8: Plot of the critical coupling as a function of temperature and chemical potential obtained after differentiating the solutions (one or two) of Eq. (3.15) and then plugging in the values of $T$, $\mu$ and $m$ into the gap equation Eq. (2.31) to get the critical coupling. The regularization parameter $\Lambda = 0.942\,\text{GeV}$. To draw the actual phase diagram, we slice Fig. 4.8 in the desired value of the coupling.

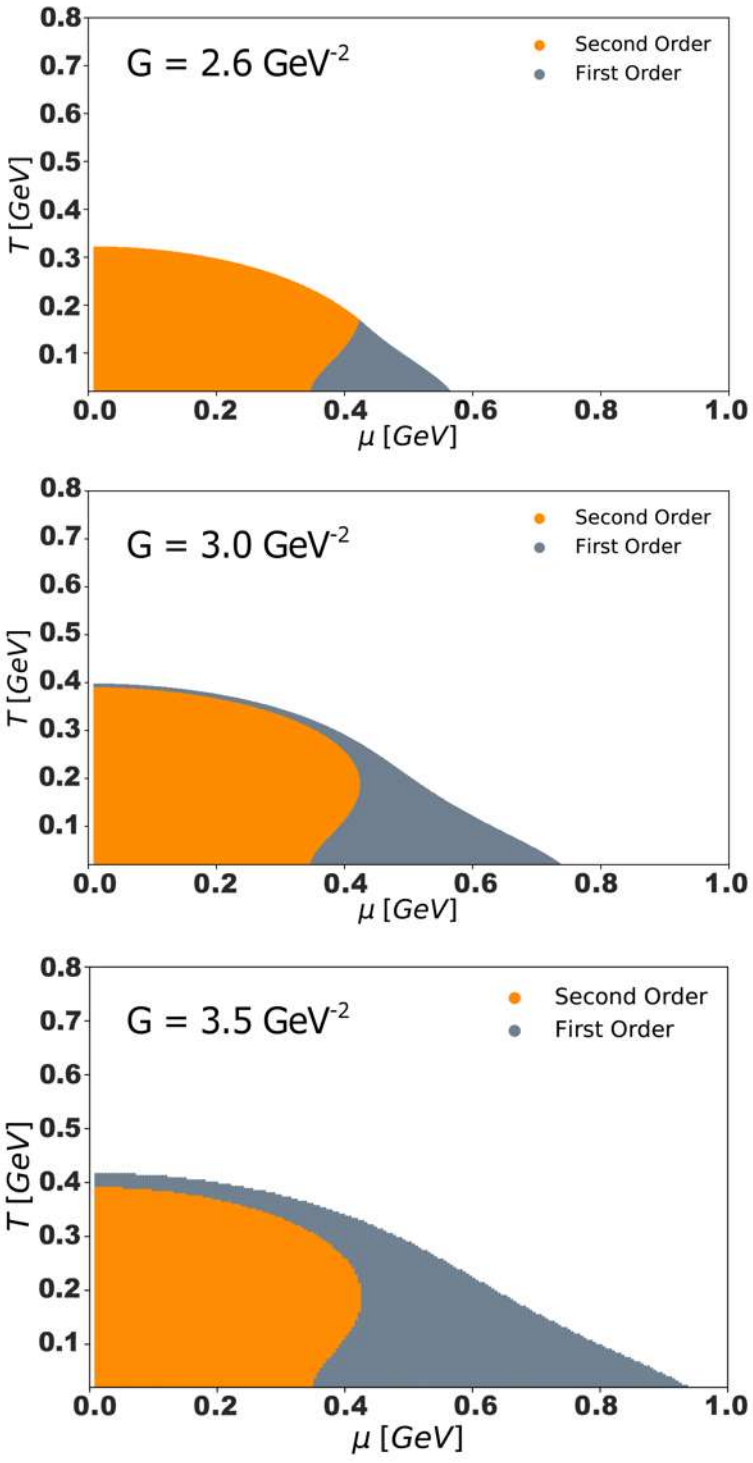


Figure 4.9: Phase diagram obtained after slicing Fig. 4.8 for $G = 2.6$ GeV$^{-2}$, $G = 3.0$ GeV$^{-2}$ and $G = 3.5$ GeV$^{-2}$. The orange area shows the second phase transition zone, whereas the gray area shows the first order phase transition zone. Notice how as the coupling becomes larger the first phase transition zone "wraps" around the second phase transition zone.

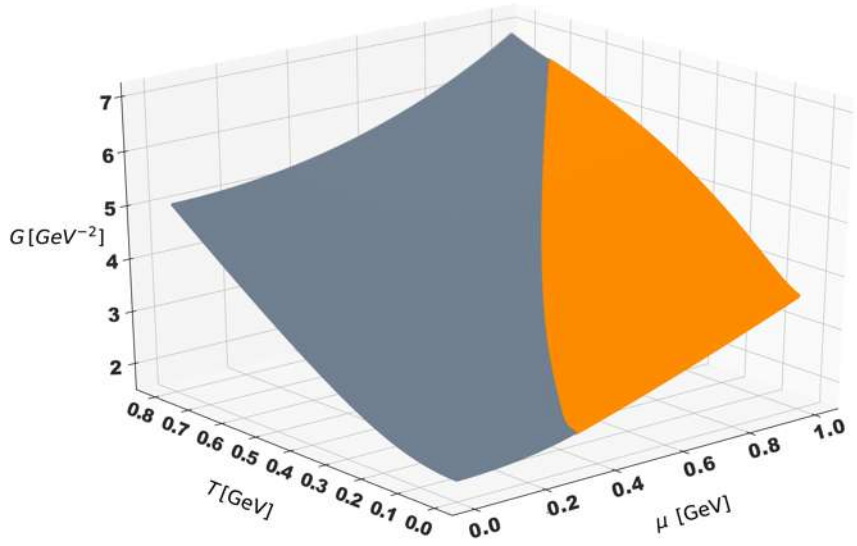


Figure 4.10: Plot of the critical coupling for the gap equation Eq. (2.31) with the medium integrals regularized. $\Lambda = 0.942\,\text{GeV}$.

we were expecting, a first and second order phase transition and the CEP located where the boundaries meet. Here, $T_{CEP} \approx 0.225$ GeV and $\mu_{CEP} \approx 0.49$ GeV. Raising the coupling further, at $G = 3.5$ GeV$^{-2}$ the transition temperature $T_{CEP} \simeq 0.513$ GeV and the critical chemical potential $\mu_{CEP} \simeq 0.94$ GeV also have raised as expected, as the coupling is so strong that is able to maintain the condensate longer albeit the high temperature and chemical potential.

## 4.6 PHASE DIAGRAM - $T_c$ AND $\mu_c$ AS BOUNDARIES

As we have seen, the election of the free parameters is crucial to drawing a phase diagram that resembles the one obtained by LatticeQCD among another methods. Following the ideas found on [22], in this Section we search for the parameters, $G$ and $\Lambda$ that replicate the values of $T_c$ and $\mu_c$ in literature. This is done by fixing the critical values of the temperature and the chemical potential in the critical condition,

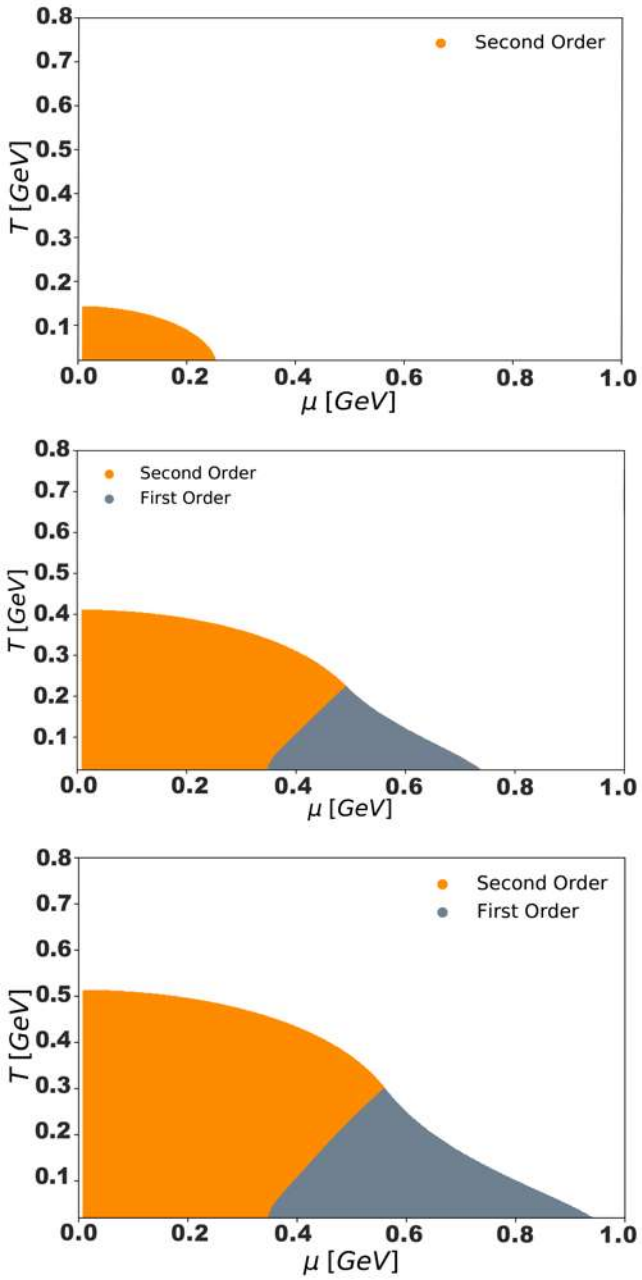


Figure 4.11: Phase diagram obtained after slicing Fig. 4.10 with $G = 2$ GeV$^{-2}$, $G = 3$ GeV$^{-2}$ and $G = 3.5$ GeV$^{-2}$. In the mid plot, $T_c \approx 0.411$ GeV and $\mu_c \approx 0.737$ GeV whereas the CEP is located at $T_{CEP} \approx 0.225$ GeV and $\mu_{CEP} \approx 0.49$ GeV. For the lower plot, $T_c \approx 0.513$ GeV and $\mu_c \approx 0.94$ GeV and the CEP is located at $T_{CEP} \approx 0.3$ GeV and $\mu_{CEP} \approx 0.56$ GeV.

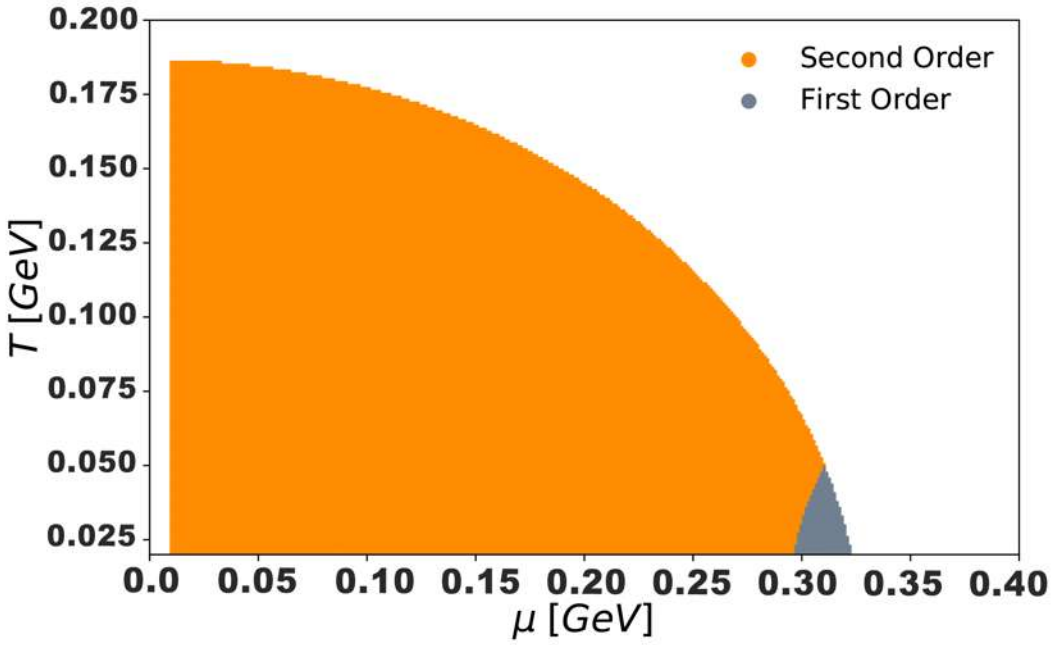


Figure 4.12: Phase diagram obtained fixing $T_c = 0.186$ GeV and $\mu_c = 0.323$ GeV in Eq. (3.15). After solving, $\Lambda = 0.8$ GeV and $G = 3.072$ GeV$^{-2}$ and the CEP is located $T_{CEP} = 0.049$ GeV and $\mu_{CEP} = 0.31$ GeV.

Eq. (3.15). This yields a systems of two equations that must be solved for the regularization parameter and coupling constant

$$\begin{aligned} \frac{d}{dm}y &= G_c \frac{d}{dm}F(m, T_0, 0, ...; \Lambda), \\ \frac{d}{dm}y &= G_c \frac{d}{dm}F(m, 0, \mu_0, ...; \Lambda), \end{aligned} \tag{4.9}$$

where $T_0$ and $\mu_0$ is the fixed values of the critical temperature and chemical potential as given by LatticeQCD. Fig. 4.12 shows the phase diagram drawn after solving Eq. (4.9) with $T = 0.186$ GeV and $\mu = 0.323$ GeV. We found $\Lambda = 0.8$ GeV and $G = 3.072$ GeV$^{-2}$ and the location of the CEP at $T_{CEP} = 0.049$ GeV and $\mu_{CEP} = 0.31$ GeV, in fair agreement with [22].

# CONCLUSIONS

# 5

# CONCLUSIONS

Although simple the NJL model can give us insights about the physics of quarks and the QCD phase diagram. Furthermore, it is the perfect playground to test new ideas to explore the phase diagram.

In this thesis we have:

- Found a condition that yield the critical coupling $G_c$ i.e. the minimum coupling that is capable of breaking the chiral symmetry.
- Extended the method to find the critical coupling using Lagrange Multipliers; this lead us to the critical condition Eq. (3.15).
- With the critical condition at hand, found the critical coupling $G_c$ for any range of values of the chemical potential and temperature and what is more, the phase diagram.

After that, applying this ideas to the NJL model, we found the critical coupling for the gap equation in a heat bath for the $3D$ cutoff and proper time regularizations, Eq. (3.10) and Eq. (4.3). If we consider solely the effect of an external magnetic field, the critical coupling condition yields a divergent critical coupling Eq. (4.4). This means the chiral symmetry is always broken no matter how small the coupling is, although the generated mass is really small. If the temperature is added to the effects of the magnetic field, the critical coupling becomes defined one again, Eq. (4.5).

We explore briefly the behavior of the critical coupling for arbitrary dimensions for the gap equation in vacuum. Eq. (4.8) and found that for $D = 2$ the necessary coupling to break chiral symmetry is zero whereas for $D = 3$ and upper dimensions, the needed coupling to trigger mass generation becomes larger as dimensions grows.

Lastly, using the critical condition Eq. (3.15) we sketched the phase diagram, first for the case where the medium integrals are not regularized. We found out that, as the coupling increases, the first order phase transition area wraps around the

second order phase transition creating a disconnection between the second order phase transition area and the unbroken phase. We point out, however, that due the very high strength of the coupling $G > 3.0$ GeV$^{-2}$, the most likely scenario is that the NJL model is unable to describe the phase diagram of QCD properly. In the second case, where the medium contribution is regularized, the wrapping does not occur for any value of the coupling.

In the last Section, we form a set of equations fixing the critical temperature $T_c$, and the critical chemical potential $\mu_c$, in the critical condition, Eq. (3.15). Solving simultaneously we were able to find a phase diagram that reproduces the location of the CEP found in recent literature [22].

# BIBLIOGRAPHY


[1] Y. Nambu and G. Jona-Lasinio. Dynamical model of elementary particles based on an analogy with superconductivity. ii. *Phys. Rev.*, 124:246–254, October 1961. DOI: 10.1103/PhysRev.124.246. URL: https://link.aps.org/doi/10.1103/PhysRev.124.246 (cited on page 5).

[2] Y. Nambu and G. Jona-Lasinio. Dynamical model of elementary particles based on an analogy with superconductivity. i. *Phys. Rev.*, 122:345–358, April 1961. DOI: 10.1103/PhysRev.122.345. URL: https://link.aps.org/doi/10.1103/PhysRev.122.345 (cited on page 5).

[3] L. X. Gutiérrez-Guerrero, A. Bashir, I. C. Cloët, and C. D. Roberts. Pion form factor from a contact interaction. *Phys. Rev. C*, 81:065202, June 2010. DOI: 10.1103/PhysRevC.81.065202. URL: https://link.aps.org/doi/10.1103/PhysRevC.81.065202 (cited on pages 5, 48, 50).

[4] Kenji Fukushima. Phase diagrams in the three-flavor Nambu-Jona-Lasinio model with the Polyakov loop. *Phys. Rev. D*, 77:114028, June 2008. DOI: 10.1103/PhysRevD.77.114028. URL: https://link.aps.org/doi/10.1103/PhysRevC.81.065202. [Erratum: Phys.Rev.D 78, 039902 (2008)] (cited on pages 5, 24).

[5] D. GÃ³mez Dumm, A. G. Grunfeld, and N. N. Scoccola. Covariant nonlocal chiral quark models with separable interactions. *Physical Review D*, 74(5):114028, September 2006. DOI: 10.1103/physrevd.74.054026. URL: http://dx.doi.org/10.1103/PhysRevD.74.054026. [Erratum: Phys.Rev.D 78, 039902 (2008)] (cited on page 5).

[6] Michael Buballa. Njl-model analysis of dense quark matter. *Physics Reports*, 407(4-6):205–376, 2005 (cited on pages 6, 24, 26).

[7] S. P. Klevansky. The nambu—jona-lasinio model of quantum chromodynamics. *Rev. Mod. Phys.*, 64(5):649–708, July 1992. DOI: 10.1103/RevModPhys.64.649. URL: https://link.aps.org/doi/10.1103/RevModPhys.64.649. [Erratum: Phys.Rev.D 78, 039902 (2008)] (cited on pages 6, 10).

[8] H. Kohyama, D. Kimura, and T. Inagaki. Regularization dependence on phase diagram in nambu–jona-lasinio model. *Nuclear Physics B*, 896:682–715, 2015. DOI: https://doi.org/10.1016/j.nuclphysb.2015.05.015. URL: http:

//www.sciencedirect.com/science/article/pii/S0550321315001753 (cited on pages 8, 10, 12).

[9] Ken-Ichi Aoki, Shinnosuke Onai, and Daisuke Sato. Analysis of Spontaneous Mass Generation by Iterative Method in the Nambu-Jona-Lasinio Model and Gauge Theories. In *KMI-GCOE Workshop on Strong Coupling Gauge Theories in the LHC Perspective*, pages 439–442, 2014. DOI: 10.1142/9789814566254_0053. arXiv: 1304.2848 [hep-th] (cited on page 11).

[10] Angelo Martínez and Alfredo Raya. Solving the gap equation of the njl model through iteration: unexpected chaos. *Symmetry 2019, 11(4), 492*, April 4, 2019. DOI: 10.3390/sym11040492. arXiv: 1904.02732 [hep-ph] (cited on pages 11, 30).

[11] Angelo Martınez and Alfredo Raya. Solving the Gap Equation of the NJL Model through Iteration: Unexpected Chaos. *Symmetry*, 11(4):492, 2019. DOI: 10.3390/sym11040492. arXiv: 1904.02732 [hep-ph] (cited on page 13).

[12] Joseph I. Kapusta and Charles Gale. *Finite-Temperature Field Theory: Principles and Applications*. Cambridge Monographs on Mathematical Physics. Cambridge University Press, 2nd edition, 2006. DOI: 10.1017/CBO9780511535130 (cited on pages 14, 15).

[13] Michel Le Bellac. *Thermal Field Theory*. Cambridge Monographs on Mathematical Physics. Cambridge University Press, 1996. DOI: 10.1017/CBO9780511721700 (cited on page 14).

[14] Ashok Das. *Finite Temperature Field Theory*. WORLD SCIENTIFIC, 1997. DOI: 10.1142/3277. eprint: https://www.worldscientific.com/doi/pdf/10.1142/3277. URL: https://www.worldscientific.com/doi/abs/10.1142/3277 (cited on pages 14, 15).

[15] Ashok K. Das. Topics in finite temperature field theory. Asoke N. Mitra, editor. April 2000. arXiv: hep-ph/0004125 (cited on page 14).

[16] E. T. Whittaker and G. N. Watson. *A Course of Modern Analysis*. Cambridge Mathematical Library. Cambridge University Press, 4th edition, 1996. DOI: 10.1017/CBO9780511608759 (cited on page 19).

[17] John Adams et al. Experimental and theoretical challenges in the search for the quark gluon plasma: The STAR Collaboration's critical assessment of the evidence from RHIC collisions. *Nucl. Phys. A*, 757:102–183, 2005. DOI: 10.1016/j.nuclphysa.2005.03.085. arXiv: nucl-ex/0501009 (cited on page 23).

[18] Jaroslav Adam et al. Enhanced production of multi-strange hadrons in high-multiplicity proton-proton collisions. *Nature Phys.*, 13:535–539, 2017. DOI: 10.1038/nphys4111. arXiv: 1606.07424 [nucl-ex] (cited on page 23).

[19] Heng-Tong Ding. New developments in lattice qcd on equilibrium physics and phase diagram, February 27, 2020. arXiv: 2002.11957 [hep-lat] (cited on page 23).

[20] Owe Philipsen. Constraining the qcd phase diagram at finite temperature and density, 2019. arXiv: 1912.04827 [hep-lat] (cited on page 23).

[21] Christian S. Fischer. QCD at finite temperature and chemical potential from Dyson–Schwinger equations. *Prog. Part. Nucl. Phys.*, 105:1–60, 2019. DOI: 10.1016/j.ppnp.2019.01.002. arXiv: 1810.12938 [hep-ph] (cited on page 23).

[22] Alejandro Ayala, L.A. Hernández, M. Loewe, Juan Cristobal Rojas, and R. Zamora. On the critical end point in a two-flavor linear sigma model coupled to quarks. *Eur. Phys. J. A*, 56(2):71, 2020. DOI: 10.1140/epja/s10050-020-00086-z. arXiv: 1904.11905 [hep-ph] (cited on pages 23, 56, 58, 62).

[23] Wei-jie Fu, Jan M. Pawlowski, and Fabian Rennecke. Qcd phase structure at finite temperature and density. *Phys. Rev. D*, 101:054032, 5, March 2020. DOI: 10.1103/PhysRevD.101.054032. URL: https://link.aps.org/doi/10.1103/PhysRevD.101.054032 (cited on page 23).

[24] Y. Maezawa, S. Aoki, S. Ejiri, T. Hatsuda, N. Ishii, K. Kanaya, and N. Ukita. Thermodynamics of two-flavor lattice QCD with an improved Wilson quark action at non-zero temperature and density. *J. Phys. G*, 34:S651–654, 2007. Yu-Gang Ma, Zhi-Yuan Zhu, En-Ke Wang, Xu Cai, Huan-Zhong Huang, and Xin-Nian Wang, editors. DOI: 10.1088/0954-3899/34/8/S65. arXiv: hep-lat/0702005 (cited on page 23).

[25] Y. Aoki, G. Endrődi, Z. Fodor, S. D. Katz, and K. K. Szabó. The order of the quantum chromodynamics transition predicted by the standard model of particle physics. *Nature*, 443(7112):675–678, October 2006. DOI: 10.1038/nature05120. URL: http://dx.doi.org/10.1038/nature05120 (cited on page 23).

[26] Tanmoy Bhattacharya et al. Qcd phase transition with chiral quarks and physical quark masses. *Phys. Rev. Lett.*, 113:082001, 8, August 2014. DOI: 10.1103/PhysRevLett.113.082001. URL: https://link.aps.org/doi/10.1103/PhysRevLett.113.082001 (cited on page 23).

[27] A. Bazavov et al. Chiral and deconfinement aspects of the qcd transition. *Phys. Rev. D*, 85:054503, 5, March 2012. DOI: 10.1103/PhysRevD.85.054503. URL: https://link.aps.org/doi/10.1103/PhysRevD.85.054503 (cited on page 23).

[28] P. Senger. Qcd matter physics at fair. *Nuclear Physics A*, 967:892–895, 2017. DOI: https://doi.org/10.1016/j.nuclphysa.2017.06.056. URL: http://www.sciencedirect.com/science/article/pii/S0375947417303172. The 26th International Conference on Ultra-relativistic Nucleus-Nucleus Collisions: Quark Matter 2017 (cited on page 23).

[29] P Senger. Probing dense qcd matter in the laboratory—the cbm experiment at fair. *Physica Scripta*, 95(7):074003, May 2020. DOI: 10.1088/1402-4896/ab8c14. URL: http://dx.doi.org/10.1088/1402-4896/ab8c14 (cited on page 23).

[30] David Tlusty. The rhic beam energy scan phase ii: physics and upgrades, 2018. arXiv: 1810.04767 [nucl-ex] (cited on page 23).

[31] Yasuyuki Akiba et al. The hot qcd white paper: exploring the phases of qcd at rhic and the lhc, 2015. arXiv: 1502.02730 [nucl-ex] (cited on page 23).

[32] Peter Senger. Studies of dense nuclear matter at nica, 2020. arXiv: 2005.13856 [nucl-ex] (cited on page 23).

[33] Peter F. Kolb and Ulrich W. Heinz. Hydrodynamic description of ultrarelativistic heavy ion collisions:634–714, May 2003. Rudolph C. Hwa and Xin-Nian Wang, editors. arXiv: nucl-th/0305084 (cited on page 23).

[34] Peter F. Kolb, Josef Sollfrank, and Ulrich Heinz. Anisotropic transverse flow and the quark-hadron phase transition. *Physical Review C*, 62(5), October 2000. DOI: 10.1103/physrevc.62.054909. URL: http://dx.doi.org/10.1103/PhysRevC.62.054909 (cited on page 23).

[35] James L. Nagle and William A. Zajc. Small system collectivity in relativistic hadronic and nuclear collisions. *Annual Review of Nuclear and Particle Science*, 68(1):211–235, 2018. DOI: 10.1146/annurev-nucl-101916-123209. eprint: https://doi.org/10.1146/annurev-nucl-101916-123209. URL: https://doi.org/10.1146/annurev-nucl-101916-123209 (cited on page 24).

[36] K. Fukushima and C. Sasaki. The phase diagram of nuclear and quark matter at high baryon density. *Progress in Particle and Nuclear Physics*, 72:99–154, 2013 (cited on page 24).

[37] David Fuseau, Thorsten Steinert, and Joerg Aichelin. Phase diagram of the Polyakov–Nambu–Jona-Lasinio approach for finite chemical potentials. *Phys. Rev. C*, 101(6):065203, 2020. DOI: 10.1103/PhysRevC.101.065203. arXiv: 1908.08122 [hep-ph] (cited on page 24).

[38] Kenji Fukushima and Vladimir Skokov. Polyakov loop modeling for hot qcd. *Progress in Particle and Nuclear Physics*, 96:154–199, September 2017. DOI: 10.1016/j.ppnp.2017.05.002. URL: http://dx.doi.org/10.1016/j.ppnp.2017.05.002 (cited on page 24).

[39] Ricardo L. S. Farias, Varese S. Timóteo, Sidney S. Avancini, Marcus B. Pinto, and Gastão Krein. Thermo-magnetic effects in quark matter: nambu-jona-lasinio model constrained by lattice qcd. *The European Physical Journal A*, 53(5), May 2017. DOI: 10.1140/epja/i2017-12320-8. URL: http://dx.doi.org/10.1140/epja/i2017-12320-8 (cited on page 24).

[40] V. A. Miransky and I. A. Shovkovy. Magnetic catalysis and anisotropic confinement in qcd. *Phys. Rev. D*, 66:045006, 4, August 2002. DOI: 10.1103/PhysRevD.66.045006. URL: https://link.aps.org/doi/10.1103/PhysRevD.66.045006 (cited on page 24).

[41] Vladimir A. Miransky and Igor A. Shovkovy. Quantum field theory in a magnetic field: from quantum chromodynamics to graphene and dirac semimetals. *Physics Reports*, 576:1–209, April 2015. DOI: 10.1016/j.physrep.2015.02.003. URL: http://dx.doi.org/10.1016/j.physrep.2015.02.003 (cited on page 24).

[42] Márcio Ferreira, Pedro Costa, and Constan ça Providência. Multiple critical endpoints in magnetized three flavor quark matter. *Phys. Rev. D*, 97:014014, 1, January 2018. DOI: 10.1103/PhysRevD.97.014014. URL: https://link.aps.org/doi/10.1103/PhysRevD.97.014014 (cited on page 24).

[43] Alejandro Ayala, C. A. Dominguez, L. A. Hernández, M. Loewe, Alfredo Raya, J. C. Rojas, and C. Villavicencio. Thermomagnetic properties of the strong coupling in the local nambu–jona-lasinio model. *Phys. Rev. D*, 94:054019, 5, September 2016. DOI: 10.1103/PhysRevD.94.054019. URL: https://link.aps.org/doi/10.1103/PhysRevD.94.054019 (cited on page 24).

[44] F. Marquez and R. Zamora. Critical end point in a thermomagnetic nonlocal NJL model. *Int. J. Mod. Phys. A*, 32(26):1750162, 2017. DOI: 10.1142/S0217751X17501627. arXiv: 1702.04161 [hep-ph] (cited on page 24).

[45] Jens O. Andersen, William R. Naylor, and Anders Tranberg. Phase diagram of qcd in a magnetic field. *Rev. Mod. Phys.*, 88:025001, 2, April 2016. DOI: 10.1103/RevModPhys.88.025001. URL: https://link.aps.org/doi/10.1103/RevModPhys.88.025001 (cited on page 43).

[46] L. McLerran and V. Skokov. Comments About the Electromagnetic Field in Heavy-Ion Collisions. *Nucl. Phys. A*, 929:184–190, 2014. DOI: 10.1016/j.nuclphysa.2014.05.008. arXiv: 1305.0774 [hep-ph] (cited on page 43).

[47] Julian Schwinger. On gauge invariance and vacuum polarization. *Phys. Rev.*, 82:664–679, 5, June 1951. DOI: 10.1103/PhysRev.82.664. URL: https://link.aps.org/doi/10.1103/PhysRev.82.664 (cited on page 43).

[48] H. L. L. Roberts, A. Bashir, L. X. Gutiérrez-Guerrero, C. D. Roberts, and D. J. Wilson. andmesons, and their diquark partners, from a contact interaction. *Physical Review C*, 83(6), June 2011. DOI: 10.1103/physrevc.83.065206. URL: http://dx.doi.org/10.1103/PhysRevC.83.065206 (cited on page 48).

[49] Dietmar Ebert, Thorsten Feldmann, and Hugo Reinhardt. Extended njl model for light and heavy mesons without thresholds. *Physics Letters B*, 388(1):154–160, November 1996. DOI: 10.1016/0370-2693(96)01158-6. URL: http://dx.doi.org/10.1016/0370-2693(96)01158-6 (cited on page 50).